

Simulated variability of the Atlantic meridional overturning circulation

Mats Bentsen^{1,2}, Helge Drange^{1,2,3,4}, Tore Furevik^{3,2}, and Tianjun Zhou⁵

¹ Nansen Environmental and Remote Sensing Center, Bergen, Norway

² Bjerknes Centre for Climate Research, Bergen, Norway

³ Geophysical Institute, University of Bergen, Norway

⁴ Nansen-Zhu International Research Centre, Beijing, China

⁵ State Key Laboratory of Numerical Modeling for Atmospheric Sciences and
Geophysical Fluid Dynamics (LASG) / Institute of Atmospheric Physics,
Chinese Academy of Sciences, Beijing, China

Corresponding author:

Mats Bentsen

Nansen Environmental and Remote Sensing Center

Edv. Griegsv. 3a

N-5059 Bergen

Norway

fax: +47 55 20 58 00

phone: +47 55 20 58 01

e-mail: mats@nersc.no

Abstract

To examine the multi-annual to decadal scale variability of the Atlantic Meridional Overturning Circulation (AMOC), a four-member ensemble with a daily reanalysis forced, medium-resolution global version of the isopycnic coordinate ocean model MICOM, and a 300-years integration with the fully coupled Bergen Climate Model (BCM), have been conducted.

The simulations of the AMOC with both model systems yield a long-term mean value of 18 Sv and decadal variability with an amplitude of 1–3 Sv. The power spectrum of the inter-annual to decadal scale variability of the AMOC in BCM generally follows the theoretical red noise spectrum, with indications of increased power near the 20-years period. Comparison with observational proxy indices for the AMOC, e.g. the thickness of the Labrador Sea Water, the strength of the baroclinic gyre circulation in the North Atlantic Ocean, and the surface temperature anomalies along the mean path of the Gulf Stream, shows similar trends and phasing of the variability, indicating that the simulated AMOC variability is robust and real.

Mixing indices have been constructed for the Labrador, the Irminger and the Greenland-Iceland-Norwegian (GIN) Seas. While convective mixing in the Labrador and the GIN Seas are in opposite phase, and linked to the NAO as observations suggest, the convective mixing in the Irminger Sea is in phase with or leads the Labrador Sea. Newly formed deep water is seen as a slow, anomalous cold and fresh, plume flowing southward along the western continental slope of the Atlantic Ocean, with a return flow of warm and saline water in the surface. In addition, fast-travelling topographically-trapped waves propagate southward along the continental slope towards equator, where they go east and continue along the eastern rim of the Atlantic.

For both types of experiments, the Northern Hemisphere sea level pressure and 2 m temperature anomaly patterns computed based on the difference between climate states with strong and weak AMOC yields a NAO-like pattern with intensified Icelandic low and Azores high, and a warming of 0.25–0.5°C of the central North Atlantic sea surface temperature (SST). The reanalysis forced simulations indicate a coupling between the Labrador Sea Water production rate and an equatorial Atlantic SST index in accordance with observations. This coupling is not identified in the coupled simulation.

1 Introduction

The stability and variability properties of the Atlantic Meridional Overturning Circulation (AMOC) have been the focus of a series of recent observational and numerical based studies. There are several reasons for the general interest in the AMOC: Time series of temperature proxies from polar ice caps and marine sediments (e.g., Bond et al. 1993; Clark et al. 2002) indicate that the North Atlantic-European region has experienced changes in the surface temperature of 5–10°C on multi-annual to decadal time scales, the last warming taking place under the transition from the last glacial maximum to the Holocene. These transitions, known as Dansgaard-Oeschger (rapid warming) and Heinrich (rapid cooling) events (Alley 1998), are generally believed to be linked to variations in the strength of the AMOC (Clark et al. 2002).

For the present day climate system, the Atlantic Ocean transports about 1.2 PW of heat poleward of 25°N, or 20–30% of the total heat flux carried by the atmosphere-ocean system at this latitude (Hall and Bryden 1982; Lavin et al. 1998; Trenberth and Caron 2001). The northward heat transport in the Atlantic Ocean contributes therefore to the anomalous mild climate over large parts of North Atlantic and Europe (e.g., Rahmstorf and Ganopolski 1999). Consequently, changes in the AMOC have the potential to change the climate in this region. The latter possibility is considered as one of the major challenges in climate change (Broecker 1997; O’Neill and Oppenheimer 2002): How stable is the AMOC to human induced greenhouse warming, and is a weakening or even a (near) collapse of the AMOC likely to occur in the near future? Model results are by no means conclusive regarding this question (Cubasch et al. 2001).

Direct observations of the strength and variability of the AMOC have not been conducted, mainly due to the 3-D basin scale extent of the circulation. In the simplest model of the system, warm and relatively saline surface waters of tropical-subtropical origin flows poleward. During the northward flow, heat is lost to the atmosphere, leading to a gradual increase of the density of these water masses. At some locations, for instance in the Greenland-Iceland-Norwegian (GIN) and Labrador Seas region (Dickson and Brown 1994), the surface water may become sufficiently dense during late winter, triggering convective mixing to intermediate or abyssal depths. These dense and cold water masses, together with subsurface water masses of polar origin flowing southward through the Fram

Strait, constitute the source waters of the southward flowing branch of the AMOC.

There is observational-based evidence for a decreasing trend in the southward flow of dense waters from the Nordic Seas (Hansen et al. 2001). A freshening of the overflow waters is also observed (Dickson et al. 2002). Since these water masses are part of the AMOC, this may suggest that the strength or the structure of the circulation is changing. However, a recent study with the Hadley Centre atmosphere-ocean general circulation model (AOGCM) indicates that this may not be the case (Wu et al. 2003). Furthermore, analysis of observed hydrography from the Atlantic sub-tropical and sub-polar gyres indicate that the AMOC-system exhibit strong variations on multi-annual to decadal time scales (e.g., Curry et al. 1998; Frankignoul et al. 2001; Curry and McCartney 2001).

A variety of model studies show decadal to multi-decadal variability modes in the strength of the AMOC. The variability modes have been explained in terms of internal ocean variability caused by interactions between the AMOC, the North Atlantic sub-polar gyre, and the transport of heat and salt into the convective mixing regions (Weaver and Sarachik 1991; Weaver et al. 1991, 1993; Delworth et al. 1993), as a coupled atmosphere-ocean mode of the Northern Hemisphere (Timmermann et al. 1998; Weaver and Valcke 1998), or as an oceanic response to atmospheric forcing (Griffies and Tziperman 1995; Delworth and Greatbatch 2000).

From AOGCMs, having increasing concentrations of greenhouse gases (some models also include scenarios of the atmospheric aerosols), a 30–50% reduction (e.g., Mann and Park 1994; Dixon et al. 1999; Wood et al. 1999; Mikolajewicz and Voss 2000), or a near stabilization (e.g., Latif et al. 2000; Gent 2001; Sun and Bleck 2001) of the AMOC are found at the end of the 21st century. Furthermore, climate simulations going beyond year 2100, usually performed with models of intermediate complexity, show generally a reduced (e.g., Stocker and Schmittner 1997) or even a complete shutdown (Rahmstorf and Ganopolski 1999; Stocker and Schmittner 1997; Schmittner and Weaver 2001) of the AMOC.

The obtained differences in the model-predicted evolution of the AMOC may have a series of explanations. First of all, it is possible that the fate of the AMOC depends on the maximum atmospheric CO₂ concentration and on the rate of CO₂ increase (e.g., Stocker and Schmittner 1997; Clark et al. 2002). This can explain some of the apparent

differences between the model integrations ending at or going beyond year 2100 since the various emission scenarios become more uncertain, and consequently diverge, with time. Furthermore, the simulated stability of the AMOC may depend on the actual model system (GCM versus model of simplified complexity), the horizontal/vertical model resolution, the parameterization of unresolved topographic features and horizontal/vertical mixing processes, the realism of the sea-ice component, the treatment of continental runoff, the ability for the model to describe the major natural climate variability modes and the climate sensitivity of the model system, the use of heat and/or fresh water flux adjustments, the actual spatial temperature and salinity distributions in key regions (especially in the convective mixing regions of the North Atlantic Ocean), and so on.

The overall aim of this study is to contribute to the general understanding of the inter-annual to decadal scale natural variability modes of the AMOC for the present-day climate state. For this, the Bergen Climate Model (BCM) system (Furevik et al. 2003; Otterå et al. 2003a,b), consisting of a modified global version of the ocean model MICOM including a dynamic-thermodynamic sea ice module, and the atmosphere general circulation model (AGCM) ARPEGE/IFS, is used. This climate model system is among the very few systems that utilizes an isopycnic coordinate ocean general circulation model (OGCM). BCM is also flexible in that arbitrary grid meshes (and consequently, arbitrary land-sea masks) can be used for the atmosphere and ocean components (Furevik et al. 2003).

To assess the simulated natural variability modes obtained by BCM with fairly uniform grid meshes, a four-member ensemble of an essential identical version of the OGCM has been integrated with atmospheric reanalysis fields (Kalnay et al. 1996) for the period 1948–1999. In the following analysis, results from both the coupled (BCM) and the ocean-only (reanalysis forced MICOM) integrations are presented, together with the corresponding observed quantities, if available. Special emphasis are put on the formation, propagation and decay of thermodynamic anomalies in the Atlantic Ocean from the equator and northwards, their influence on the AMOC, and vice versa. It is clear from the complexity and the still incomplete theoretical understanding of the system (e.g., Jayne and Marotzke 2001; Johnson and Marshall 2002), that in-depth studies involving theoretical and observational analysis, together with (simplified and complex) model studies, are required to significantly improve our understanding of the AMOC.

The main motivation of the study is based on the believe that better knowledge of the present-day system has the potential to reduce the uncertainty in climate change predictions in general, and for the Atlantic-European climate system in particular. In addition, improved understanding of the major natural variability modes is a prerequisite for performing – if possible – multi-annual to decadal predictions of the Atlantic-European climate.

The paper is organized as follows: Section 2 describes the model system used for the simulations presented here. As the AOGCM has been documented in a separate paper (Furevik et al. 2003), most of the section is devoted to the description of the OGCM experiments. Section 3 presents the model results. Focus is put on the simulations of the deep convective mixing and the AMOC. Both surface forcing in the convective mixing regions and basin-scale response to the deep convective mixing are addressed. In section 4, comparison with observation based indices are presented and the various findings discussed. Other model studies concerning AMOC variability are also discussed. Section 5 concludes the paper.

2 Model system

The model system applied in this study consists of the MICOM (Miami Isopycnic Coordinate Ocean Model) OGCM (Bleck et al. 1992), a sea-ice module consisting of the Hibler III (1979) rheology in the implementation of Harder (1996) and the thermodynamics of Drange and Simonsen (1996), and the ARPEGE/IFS (Action de Recherche Petite Echelle Grande Echelle/Integrated Forecast System) AGCM (Déqué et al. 1994). The coupling of the atmosphere-sea ice-ocean model components is controlled by a modified version of the OASIS (Ocean Atmosphere Soil Sea Ice) software described by Terray and Thual (1995); and Terray et al. (1995).

2.1 The Bergen Climate Model

A general description of BCM is given in Furevik et al. (2003), and only a brief outline is given here. The AGCM is run with a horizontal resolution of T_L63 (2.8° along the equator) on a reduced gaussian grid, with 31 layers in the vertical. The atmospheric

concentration of CO₂ is held fixed at 353 ppm, whereas aerosol particles are held constant, consistent with the present day values. The OGCM and sea-ice components in BCM are identical to those of the ocean-only integrations described below, with the exception that the horizontal grid has a 2.4° resolution along the equator with one pole over Siberia and the other over the South Pole. The grid cells are approximately square except in a band along the equator where the meridional grid spacing is gradually increased to 0.8° to allow the equatorial-confined dynamics to evolve in the system.

In the BCM simulation presented here, sea-surface salinity (SSS) and sea-surface temperature (SST) are flux adjusted based on annual repeated heat and fresh water fluxes diagnosed as weekly averaged fields from the spin-up integration of the coupled system (Furevik et al. 2003). Continental run-off is distributed to the appropriate coastal grid cells of the OGCM. The global mean SST and SSS fields show a climate drift of 0.14° C and 0.03 psu over 100 years. This drift is comparable to the drift of most of the coupled models participating in the coupled model intercomparison project (CMIP) (Covey et al. 2003).

2.2 The OGCM

2.2.1 General features

For the ocean-only integrations, the MICOM OGCM was configured with a local horizontal orthogonal grid system with one pole over North America and one pole over western part of Asia (Bentsen et al. 1999). The horizontal resolution is 60–80 km over the entire North Atlantic region between 30–60°N. Another integration with doubled horizontal resolution has also been conducted. The overall features from the latter integration are consistent with the 60–80 km resolution results presented here, although local differences exist. A third integration with four times the resolution is presently under way.

The OGCM has 24 layers in the vertical, of which the uppermost mixed layer (ML) has a temporal and spatial varying density. The specified potential densities of the subsurface layers are chosen to ensure proper representation of the major water masses in the North Atlantic/Nordic Sea region. The densities of the isopycnic layers are listed in Table 1.

Table 1

The vertically homogeneous ML utilizes the Gaspar et al. (1990) bulk parameteriza-

tion for the dissipation of turbulent kinetic energy, and has temperature, salinity and layer thickness as the prognostic variables. In the isopycnic layers below the ML, temperature and layer thickness are the prognostic variables, whereas salinity is diagnostically determined by means of the simplified equation of state of Friedrich and Levitus (1972). If an isopycnic layer is lighter than the ML, convective mixing is parameterized by instantaneously transferring the mass from the isopycnic layer into the ML and mixing the dynamic and thermodynamic variables within the deepened ML. The bathymetry is computed as the arithmetic mean value based on the ETOPO-5 data base (Data Announcement 88-MGG-02, Digital relief of the Surface of the Earth, NOAA, National Geophysical Data Center, Boulder, Colorado, 1988).

The thermodynamic module incorporates freezing and melting of sea-ice and snow covered sea-ice (Drange and Simonsen 1996), and is based on the thermodynamics of Semtner Jr. (1976); Parkinson and Washington (1979); and Fichefet and Gaspar (1988). The dynamic part of the sea-ice module follows the viscous-plastic rheology of Hibler III (1979), where sea-ice is considered as a two-dimensional continuum. The dynamic ice module has been further modified by Harder (1996) to include description of sea-ice roughness and the age of sea-ice, and utilizes the positive definite advection scheme of Smolarkiewicz (1984).

The continuity, momentum and tracer equations are discretized on an Arakawa C-grid configuration (Arakawa and Lamb 1977). The diffusive velocities (diffusivities divided by the size of the grid cell) for layer interface diffusion, momentum dissipation and tracer dispersion are 0.02 m s^{-1} , 0.025 m s^{-1} and 0.015 m s^{-1} , respectively, yielding actual diffusivities of about $10^3 \text{ m}^2 \text{ s}^{-1}$. A flux corrected transport scheme (Zalesak 1979; Smolarkiewicz and Clark 1986) is used to advect the model layer thickness and the tracer quantities.

The diapycnal mixing coefficient is parameterized according to the Gargett (1984) expression $K_d = C N^{-1}$, where $C = 3 \times 10^{-7} \text{ m}^2 \text{ s}^{-2}$ and $N = (g\rho^{-1}\partial\rho/\partial z)^{1/2}$ is the Brunt-Väisälä frequency (g is the gravitational acceleration, ρ is the density, and z is the depth). The numerical implementation of the diapycnal mixing follows the scheme of McDougall and Dewar (1998).

2.2.2 Ocean-only spin-up and forcing

For the ocean-only simulations presented here, the model was initialized by the January Levitus and Boyer (1994) and Levitus et al. (1994) climatological temperature and salinity fields, respectively, a 2 m thick sea-ice cover based on the climatological sea-ice extent (Gloersen et al. 1992), and an ocean at rest. The model was then integrated for 150 years by applying the monthly mean NCEP/NCAR reanalysis fields (Kalnay et al. 1996), and thereafter forced with daily reanalysis fields twice for the five year period 1974–1978. The parameterization of surface fluxes using the NCEP/NCAR reanalysis fields is described in Bentsen and Drange (2000).

During the first 150 years of the integration, the ML temperature and salinity were relaxed towards the monthly-mean climatological values of respectively Levitus and Boyer (1994) and Levitus et al. (1994). The relaxation is carried out by applying fluxes of heat and salt proportional to the SST and SSS differences between model and climatology, respectively. The e-folding relaxation time scale was set to 30 days for a 50 m thick model ML, and it was increased linearly with ML thicknesses exceeding 50 m. No relaxation was applied in waters where sea-ice is present in March in the Arctic and in September in the Antarctic to avoid relaxation towards temperature or salinity outliers in the poorly sampled polar waters. In addition, the mismatch between model and climatology were limited to $|\Delta\text{SST}| < 1.5 \text{ }^\circ\text{C}$ and $|\Delta\text{SSS}| < 0.5 \text{ psu}$ in the computation of the relaxation fluxes. This e.g. avoids extreme fluxes in the vicinity of the western boundary currents which are not realistically separated from the coast with the current model resolution. Continental run-off is included by adding fresh water into the appropriate coastal grid cells (Furevik et al. 2003).

For the integrations presented here, annually repeated heat and fresh water relaxation fluxes with weekly temporal resolution were added to the ML. In this way, temperature and salinity anomalies are free to evolve and propagate, whereas the mean thermodynamic state is kept fairly unchanged. It was found that such a procedure is of special importance for the SSS field, indicating problems with the forcing (either the prescribed NCEP/NCAR precipitation or run-off fields, or the computed evaporation field), or inherent model deficiencies in the representation of for instance horizontal advection processes or vertical mixing of the surface waters. The weekly heat and fresh water relaxation fluxes

were diagnosed from the last 5 years of the spin-up integration. For this period, daily forcing fields for the period 1974–1978 were applied. The period was chosen as it represents a fairly neutral state of the North Atlantic Oscillation (NAO). The first NCEP/NCAR model integration was then initialized from the ocean end state of the 160 years spin-up integration.

2.3 Model integrations

Two types of model integrations are performed: A 300 years control integration with the BCM in the setting described above, and a total of four integrations with the uncoupled OGCM, forced with daily NCEP/NCAR reanalysis fields for the period 1948–1999. For the latter integrations, the ensemble members differ by different initial conditions only: Member two is initialized from year 1976 of member one, member three is initialized from the ending state (year 1999) of member one, and member four is initialized from the ending state of member three. The ocean-only integrations yield a total of 208 model years.

3 Model results

3.1 The simulated AMOC

A common diagnostics for the AMOC is the strength of the overturning, either extracted within a certain latitude-depth interval, or at a fixed latitude. In the upper panel of Fig. 1, the simulated annual mean AMOCs (in $Sv=10^6 \text{ m}^3 \text{ s}^{-1}$) from the ocean-only integrations in the latitude band 20°N – 50°N are shown for the period 1948–1999. Irrespective of the initial conditions, the AMOCs show the same trend and variability after an adjustment time of 5–10 years (this result also holds for the conducted integration with doubled horizontal resolution). In particular, the model realizations yield minima round year 1960 and 1980, maxima round 1975 and 1995, and a gradual increasing trend from 1960 to 1995.

Decadal scale variability is also found in the 300 years BCM simulation (lower panel of Fig. 1). From the coupled integration, variability modes on longer time scales are also present. Whether these modes are real or are caused by deficiencies of the coupled

Figure 1

system, is hard to assess. However, the focus of this study is on decadal scale variability, so the long term variability has been filtered in most of the analysis presented here.

Figure 2

The leading mode of the variability in the simulated AMOC is displayed in Fig. 2 as the first Empirical Orthogonal Function (EOF) and the corresponding Principal Component (PC) of the overturning stream function. The leading EOF of the ensemble mean of the ocean-only and the coupled integrations explain 79% and 57% of the variance, respectively. Differences between the obtained EOF patterns, although fairly similar, could be related to the positive trend in the AMOC in the ocean-only runs, whereas both increasing and decreasing AMOC periods are present in the coupled system. The leading PCs have a simultaneous correlation of 0.97 and 0.86 with the strength of the AMOC in the ocean-only and BCM experiments, respectively. Consequently, PC1 of the AMOC is an excellent proxy for the intensity of the basin scale overturning. In von Storch et al. (2000), the leading EOF of the Atlantic overturning stream function is computed using four 1000 year integrations performed with different AOGCMs. The four EOFs explains the variance by 41–56%, and the corresponding PC's have maximums in the range 1.6–2.4 Sv. It is most meaningful to compare these results with the EOF of our 300 year coupled integration, and this reveals that we get a structure very similar (but slightly weaker) to the structure obtained from three out of the four integrations presented in von Storch et al. (2000).

3.2 Convective mixing indices

Figure 3

The power spectrum of PC1 of the overturning stream function in BCM is displayed in Fig. 3, together with an estimated theoretical red noise spectrum. Compared to the red noise spectrum, the PC1 spectrum has less energy at periods 3.5–7 years, elsewhere it generally follows the red noise spectrum. Some increased power is found near the 20 year period. As the focus of this study is on multi-annual to decadal time scales, the following analysis will be based on time periods larger than 5 years. In addition, the analysis of the BCM integration has been limited to time scales less than 100 years to remove most of the long-term variability seen in the lower panels of Figs. 1 and 2.

It is well established that there is a clear correspondence between formation of intermediate to deep waters in the North Atlantic and the AMOC (e.g., Mauritzen and

Häkkinen 1999; Eden and Jung 2001; Curry and McCartney 2001). In the following, three deep-water formation sites in the North Atlantic Ocean are identified and examined, and thereafter linked to the variability in the simulated AMOC.

Figure 4

The locations of the convective mixing in the ocean-only integrations and the BCM simulation are fairly similar (Fig. 4), and are found in the Labrador, Irminger and GIN Seas. The classical picture is that deep convective mixing takes place in the Labrador and the GIN Seas, but not in the Irminger Sea. However, as pointed by Pickart and Lavender (2000) and Pickart et al. (2003), historical and recent observations indicate that the Irminger Sea is a region of deep convective mixing. This is also the case for the modelling results presented here.

Figure 5

Convective mixing indices are constructed as the normalized mean February to April (FMA) ML volume in the areas where the FMA ML depth exceeds 1500 m at least once during the actual integration (the shaded areas in Fig. 4). In Fig. 5, the monthly mean ML thickness for the Labrador, Irminger and GIN Seas are shown. The maximum ML is between 100 and 200 m deeper in the BCM experiment compared to the ocean-only integrations, but otherwise very similar. For both types of model experiments, the convective mixing penetrates deepest in the Irminger and GIN Seas (1000–1400 m on average), whereas there is mixing to 600–800 m in the Labrador Sea.

Since the focus of this paper is on the natural variability of the AMOC, the interannual variability of the ML is as important as the actual convective mixing depths. The variability of the ML depth, represented as year-to-year standard deviation for each month, is plotted in the lower panels of Fig. 5. It is seen that for both the ocean-only and the BCM experiments, the ML variability in the Labrador Sea exceeds that of the Irminger Sea by 100–150 m. Furthermore, the GIN Sea ML variability is largest in the ocean-only simulations. The latter could be linked to the extreme change in the NAO-forcing over the last 50 years, and a generally weaker vertical density stratification in the GIN Seas than in the Labrador Sea.

The general agreement between the ocean-only and coupled experiments with respect to the location of the convective mixing regions, the annual cycle in the mixing depths and, with the exception for the GIN Seas, the temporal variability of the mixing, suggests that the overall structures of the convective mixing in the two types of model experiments

are consistent and comparable.

3.3 Cross-correlations

Figure 6

Cross-correlations between the obtained convective mixing indices for the Labrador, Irminger and GIN Seas are displayed in Fig. 6. For both types of model experiments, maximum correlation exists between the convective mixing in the Labrador and Irminger Seas, with a tendency for convective mixing in the Irminger Sea to lead that of the Labrador Sea. In addition, the convective mixing in the Labrador and the GIN Seas is significantly anti-correlated, at zero time lag.

Figure 7

The switching of the convective mixing between the Labrador and the GIN Seas is also seen in hydrographic observations for the last 50 years (Dickson et al. 1996), with deeper (weaker) than normal mixing in the Labrador Sea when the NAO index is high (low). The correspondence between convective mixing and the leading PC of the Northern Hemisphere sea-level pressure (SLP) is plotted in Fig. 7, showing that the Labrador Sea mixing (and for the ocean-only integrations, the Irminger Sea mixing) vary in accordance with the leading mode of the Northern Hemisphere SLP (NAO). The convective mixing in the GIN Seas is anti-correlated with the strength of the NAO in the coupled simulation while this is not that obvious in the ocean-only simulations.

Figure 8

The cross-correlation between the convective mixing indices and PC1 of the AMOC is shown in Fig. 8. It follows that the decadal scale variabilities of the AMOC are not strongly related to the simulated deep-water formation in the GIN Seas at the 95% confidence level. This finding is in accordance with the study of Mauritzen and Häkkinen (1999). However, for both experiments, convective mixing in the Labrador and Irminger Seas leads to an intensified AMOC with lags of 0–5 years, with a tendency for the Irminger Sea mixing to take place a few years prior to the onset of the Labrador Sea mixing.

3.4 Surface forcing

Furevik et al. (2003) found that the NAO mode of variability is captured by the coupled model, with realistic frequency distribution and area of influence. It is well established that there is a strong link between the NAO and the formation of Labrador Sea Water

(LSW), and subsequently on the AMOC (e.g., Curry and McCartney 2001; Eden and Jung 2001). However, several of the observed and simulated multi-annual to decadal scale variability modes can not easily be described in terms of a passive response to NAO (Dong and Sutton 2001). To examine the simulated ocean response to the atmospheric forcing in the two types of experiments presented here, the Labrador and the Irminger Seas convective mixing indices have been lag correlated with the total heat flux and the associated SLP anomalies. It turns out that both types of model experiments show near identical lag correlations. Therefore, only the lag correlations obtained from the BCM experiment is shown here.

Figure 9

The obtained results for the Labrador Sea for zero time lag are displayed in Fig. 9.

Figure 10

From these panels, the classical NAO forcing pattern with the three-pole total heat flux and the dipole NAO type SLP distributions are apparent (Marshall et al. 2001). Consequently, the formation of LSW is tightly related to the NAO forcing in BCM (and in the ocean-only integrations; see also Fig. 7).

Figure 11

The situation for the convective mixing in the Irminger Sea is different, however, as seen in Fig. 10. Here the deep convection is associated with lower than normal SLP over the southern part of the Nordic Seas leading to anomalously strong northerly winds over the Irminger Sea. Associated with this, the North-East Atlantic experiences cooling. The model experiments therefore indicate that convective mixing in the Labrador Sea is related to atmospheric forcing that resembles the NAO pattern, whereas the Irminger Sea mixing is mainly associated with a situation with locally increased northerly winds.

That the convective mixing indices of the Labrador and Irminger Seas may or may not act in concert is demonstrated in Fig. 11. It follows that regimes exist where the two mixing indices act together, leading to an intensified/weakened AMOC, or that they evolve in different directions, leading to a reduced/cancelled effect on the AMOC.

Lag correlation plots for the total fresh water flux and the convective mixing indices have also been generated. It was found that changes in the fresh water forcing did not correlate with the three indices, and these results are therefore not shown.

3.5 Localized responses to convective mixing anomalies in the sub-polar region

Lag correlations along vertical sections are a powerful diagnostics to examine the formation, propagation and decay of thermodynamic and dynamic anomalies. Here we present density, temperature, salinity and velocity anomaly correlations with respect to the leading PC of the AMOC from the BCM integration along two sections: One section follows the western continental slope of the Atlantic Ocean, and the other the 48°N parallel (Fig. 12).

Figure 12

The corresponding fields from the ocean-only integrations resemble those presented here, and are therefore not displayed.

For the section along the western continental slope (Fig. 13), density anomalies caused by temperature, and to some extent by salinity, form at lag of +6 to +4 years in the sub-polar gyre. These anomalies grow with time, and a deep southward propagating signal is seen as cold, fresh and dense water. From the velocity panels, it follows that the southward flow of dense water is compensated by a northward velocity anomaly. It is also seen that the surface water density anomaly disappears at lags < -2 years, and that this is caused by warm and saline surface waters, with the former overcompensating the effect on density compared to the latter.

Figure 13

Figure 14

In the section along 48°N (Fig. 14), the deep southward propagating signal is clearly seen as a plume of cold and fresh water. Furthermore, the velocity response has a baroclinic structure with a northward component over the uppermost 2000 m of the water column in the western part of the basin. The northward component carries warm and saline waters, leading to a negative density anomaly there. The reduced density of the northward surface and near surface flow tends to inhibit convective mixing when these waters reach the sub-polar gyre. This is also shown in the density panels of Fig. 13 at lag -2 and -4 years. In this way, the previous convective mixing event can generally not be maintained over time due to the high temperature of the northward flowing surface waters. At the same time, the accompanying supply of saline surface waters acts as a preconditioning factor for the following convective mixing event when the surface water becomes sufficiently cooled.

3.6 Basin-scale responses to variations in the AMOC

Figure 15

The barotropic responses to the variations in PC1 of the BCM AMOC are displayed in Fig. 15 (the results from the ocean-only integrations are very similar, and therefore not shown). It follows from the panels in Fig. 15 that associated with the deep convective mixing in the Irminger and Labrador Seas prior to maximum AMOC, there is an intensification of the sub-polar gyre circulation. Maximum response (correlation > 0.6) is found two years prior to maximum AMOC. In addition, the barotropic stream function of the northward part of the sub-tropical gyre correlates positively with PC1 of the AMOC. The latter finding is consistent with a northward displacement, and also an intensification, of the Gulf Stream system. Therefore, positive SST and SSS anomalies are found in the region of the intensified Gulf Stream system as is seen in Fig. 14.

A striking feature in Fig. 15 is a fast propagating positive anomaly along the western boundary of the Atlantic Ocean. When the anomaly reaches the equator, it propagates along the equator, before disappearing. The propagating speed associated with this feature far exceeds the advective speed with an estimated value of 0.02 to 0.04 m s^{-1} based on Lagrangian observations (Bower and Hunt 2000). The simulated feature is similar in structure and characteristics to coastally trapped baroclinic (Kelvin) waves, initiated by the newly formed intermediate to deep water masses in the sub-polar gyre, as discussed in e.g., Kawase (1987); Yang (1999); Johnson and Marshall (2002). When the Kelvin waves reach the eastern coast at the equator, they propagate northwards and southwards along the coast, radiating Rossby waves westward into the ocean interior, and gradually disappears (Johnson and Marshall 2002).

Figure 16

Since the layer interfaces in an isopycnic coordinate OGCM can be viewed as material surfaces (with the exception of the applied diapycnal mixing), a model with this choice of vertical coordinate is well suited for studying propagation of anomalies manifested in the layer interface depths. It is therefore not surprising that the same structure is found in the lag correlation between PC1 of the AMOC and the $\sigma_0 = 27.71$ interface depth as shown in Fig. 16. A positive anomaly is formed in the convective locations in the sub-polar gyre at lags +6 to 0 years, and thereafter propagates southward along the western rim of the Atlantic. At lag -2 years, the anomaly reaches the equator, and continues eastward along the equator. At lag -4 years, a weakened anomaly is seen northward along the eastern

coast. There are also indications of signals that radiate back into the ocean interior from the eastern coast, both findings in general accordance with the wave propagation theory mentioned above. It should also be noted that for lags exceeding 2 years, the sub-tropical and equatorial Atlantic correlates negatively with the PC1 of the AMOC. All of these changes are significant at the 95% level.

Based on hydrographic observations for the period 1945–1993, Yang (1999) showed that an equatorial dipole index, defined as the difference between northern (0–20°N) and southern (0–20°S) Atlantic SSTs, correlates with the observed thickness variations of the LSW with a lag of about –5 years (correlation coefficient was +0.68). Yang (1999) argues, and also shows by means of an idealized set-up of a z -level OGCM, that the equatorial SST structure is a consequence of the variability of the LSW about 5 years prior to the occurrence of the equatorial SST dipole.

The analysis of Yang (1999) have been repeated based on the ocean-only and the BCM experiments. The results obtained from the ocean-only integrations are displayed in Fig. 17. For a time lag of 6 years (in contrast to the 5 years lag proposed by Yang (1999)), there is a tight correspondence between the simulated LSW production rate and the equatorial SST dipole. It should be noted that in the ocean-only integrations, the tropical dipole index follows the NCEP/NCAR reanalysis closely, and is not an independent feature.

Figure 17

Interestingly, a similar lag-correlation is not found in the BCM experiment (not shown), despite the significant dynamical response in the equatorial region as shown in Figs. 15 and 16. This will be discussed in the next section.

4 Discussion

The presented model experiments indicate that a direct comparison between the simulated AMOC and the North Atlantic Oscillation (NAO) index of e.g. Hurrell (1995) show some, but a far from conclusive, correspondence between the two quantities (e.g., section 3.4). However, the simulated AMOC minima in 1960 and 1980, and the maxima round 1975 and 1995, resemble observed variations of the core thickness of LSW (Curry et al. 1998). Correspondingly, the variability of the simulated AMOC is fairly consistent with the At-

Figure 18

lantic transport index proposed by Curry and McCartney (2001) representing the strength of the baroclinic gyre circulation in the North Atlantic Ocean (top panel in Fig. 18).

Another type of proxy which is thought to be linked to the AMOC (Frankignoul et al. 2001; Rossby and Benway 2000) is the Gulf Stream indices by Taylor and Stephens (1980) and Joyce et al. (2000). The first of these indices represents the north-south movement of the core of the Gulf Stream water as it leaves the American coast near Cape Hatteras, whereas the second index represents the temperature anomalies along the mean Gulf Stream path. The latter index, based on the variability in the simulated SST field as described in conjunction with Fig. 4 of Frankignoul et al. (2001), is computed for all four ocean-only simulations and is displayed in the mid panel of Fig. 18. The ensemble mean of these indices is in general agreement with the Joyce et al. (2000) index (Fig. 18, lower panel).

From the presented comparisons with the observational based transport index of Curry and McCartney (2001) and the Gulf Stream index of Joyce et al. (2000), we conclude that the overall phasing of the simulated decadal scale AMOC variability, and the obtained trend from 1960 to 1995, are robust results, at least for the applied OGCM. The actual amplitude of the decadal scale variability modes and the slope of the trend are, however, hard to assess based on comparison with observational based indices. Model studies carried out with z -level OGCMs (e.g., Eden and Jung 2001) yield similar results, indicating that these conclusions are not model dependent.

Furthermore, the general similarity between the ocean-only integrations and the BCM experiment lead us to conclude that the simulated multi-annual to decadal variability is independent of the two model configurations. The major exception to this statement is the failure of BCM to reproduce the coupling between the AMOC and the tropical dipole index. There could be several reasons for this discrepancy: Another study (Frankignoul et al. 2003) indicates that in the coupled model the heat flux feedback is too strong and the SST anomalies are too short-lived in the tropical Atlantic compared to observations, or that the second half of the 20th century (the period with observational data) is untypical due to greenhouse gas forcing, the possibly related gradually strengthening NAO, or other factors. Continued observations of the convective mixing in the sub-polar region and of the equatorial Atlantic SST, analysis of other coupled models, and possibly im-

provements of BCM's performance in the tropical Atlantic, are needed to assess these questions. Provided the results of Yang (1999) are representative and robust, it follows that the sub-polar convective mixing and the Atlantic tropical SST variations are linked through the AMOC, and that this link can feed back to the atmospheric circulation through anomalous heat fluxes in the tropics with a time lag of 5–6 years.

A series of studies with OGCMs (Weaver and Sarachik 1991; Weaver et al. 1991, 1993) show variability of the AMOC caused by internal ocean processes. In these studies, the OGCMs are driven by wind, restoration of sea surface temperature (SST) to prescribed values, and specified freshwater fluxes (mixed boundary conditions). It is concluded based on the studies that the specification of the freshwater forcing is the dominant factor in determining the models internal variability.

Delworth et al. (1993) finds, using an AOGCM, irregular oscillations of the AMOC with a time scale of approximately 50 years. They explain this as a primarily ocean-only mode of variability, which arises from the interplay of the AMOC, the North Atlantic subpolar gyre circulation, and the transport of heat and salt into the main sinking region of their model. Using a box-model for the ocean, Griffies and Tziperman (1995) found decadal scale variability of the overturning circulation when their model was driven by stochastic atmospheric forcing. The variability was explained as a damped oscillatory mode. Weisse et al. (1994) describes a similar damped oscillatory mode of the AMOC by stochastically forcing an OGCM.

A decadal time scale coupled atmosphere-ocean mode of the Northern Hemisphere is described by Timmermann et al. (1998). This mode involves the AMOC and its interaction with the atmosphere in the North Atlantic and interactions between ocean and atmosphere in the North Pacific. Weaver and Valcke (1998); Delworth and Greatbatch (2000) addressed the conflicting explanations of the AMOC variability by investigating several OGCM simulations with different atmospheric forcing. Both studies excluded the variability as an ocean-only feature. Weaver and Valcke (1998) concluded that the decadal AMOC variability is a mode of the full coupled system, while Delworth and Greatbatch (2000) found that the variability should largely be viewed as an oceanic response to the atmospheric forcing, although air-sea coupling appears to modify the amplitude of the variability.

The similarity between the two types of model experiments presented here (ocean-only vs. coupled model) supports the view that the decadal scale variability of AMOC is a response to atmospheric forcing, a forcing that is associated with pressure anomalies in the vicinity of Iceland and the Azores.

The presented results have focussed on the formation, propagation and decay of thermodynamic and dynamic anomalies in the Atlantic Ocean. A major challenge for climate research is to assess the degree of predictability of the Atlantic-European climate, and consequently, to understand mechanisms for possible coupling modes between the AMOC and atmospheric circulation regimes (e.g., Bjerknes 1964). This aspect has not been explicitly addressed here.

However, it follows from section 3.3 that the Labrador Sea convective mixing index correlates with the leading mode of the Northern Hemisphere SLP at zero time lag, and with the AMOC at zero to 5 years time lag. The spatial structure of the SLP and the 2 m temperature anomaly fields for the composite of years with strong minus years with weak AMOC are shown in Fig. 19. The obtained SLP pattern is similar to the classical NAO-pattern with centers of action in the vicinity of Iceland and the Azores. It follows that the pressure difference is increased on average by 5 mbar in years with strong compared to weak AMOC. The corresponding 2 m temperature response gives a warming over the central North Atlantic of 0.25–0.5°C, and a cooling of the same magnitude in a region extending eastward of the Azores. A mechanistic understanding of these responses, possibly together with the tropical dipole SST pattern discussed in section 3.6, are needed to better understand the coupling between the atmosphere and ocean systems on multi-annual to decadal time scales.

Figure 19

5 Conclusions

The surface temperature of large parts of the North Atlantic-European region is exceptionally high compared to the corresponding zonal mean, at least partly caused by the loss of heat from the Gulf Stream-North Atlantic Drift systems. Climate proxies from ice cap and ocean sediment cores show that the region has experienced a series of excessive and rapid cooling events, possibly linked to a significant reduction in the strength of the

AMOC. It is also speculated that continued human induced pollution of the atmosphere may lead to a reduced, or even to a near total collapse, of the AMOC.

Here we present results from four 52 years integrations with the isopycnic coordinate OGCM MICOM, and one 300 years control integration with the Bergen Climate Model consisting of MICOM coupled to the AGCM ARPEGE/IFS.

It is shown that the ocean-only and coupled integrations are generally very similar. It is found that the multi-year to decadal scale variability in the AMOC is governed by convective mixing in the Labrador and the Irminger Seas. Apparently, the GIN Seas region does not play an active role, at least on the time scales addressed here. It is further found that the formation of intermediate to deep water masses in the Labrador Sea is mainly determined by the NAO-forcing, whereas convective mixing in the Irminger Sea is mainly found after periods with enhanced local northerly (and cold) wind anomalies. Peak AMOC typically occurs 2–4 years after the occurrence of convective mixing events in the sub-polar region. It is further demonstrated that the AMOC could remain almost unchanged if the convective mixing anomalies in the Labrador and Irminger Seas have different sign. It is therefore the net effect of the two contributions that force the multi-annual to decadal scale anomaly of the AMOC in the model systems presented here. This result is of potential importance for monitoring of the system as convective mixing indices from the Labrador Sea may not necessarily pick up all of the major variability modes of the AMOC.

Two distinct responses follow the deep convective mixing along the continental slope of the West Atlantic Ocean: A slow advection of a deep plume of cold and fresh water, and a fast wave signal. It is found that the latter signal reaches the equator in a few years. Comparison with theoretical work and modelling with idealized OGCMs indicate that the wave signal is a topographically-trapped wave that travels southward, then eastward near the equator, and finally northward and southward along the eastern rim of the Atlantic coast, from where Rossby waves radiates into the ocean interior.

From the ocean-only integrations, high positive correlations are found between the variability of the AMOC and a tropical SST dipole at a time lag of about 6 years. This correlation is consistent with observations for the last 50 years, and is also consistent with idealized model experiments. This correspondence is, however, not present in the BCM

experiment. Consequently, the difference between the two model experiments need to be sorted out.

It is further shown that for both types of experiments, the Northern Hemisphere SLP and 2 m temperature anomaly patterns computed based on the difference between climate states with strong and weak AMOC yields a NAO-like pattern with intensified Icelandic low and Azores high, and a warming of 0.25–0.5°C of the central North Atlantic SST. These correlations, together with the tropical dipole anomaly, are two potential candidates for the signature of coupled ocean-atmosphere modes in the Atlantic Ocean. Further work is needed to address this possibility.

Acknowledgements. The model development and analysis have been supported by the Research Council of Norway through several projects, and in particular RegClim, NO-Clim and KlimaProg's "Spissforskningsmidler", and the Programme of Supercomputing. The work has also received support from the EU-project PREDICATE (EVK2-CT-1999-00020). The authors would like to thank C. Frankignoul and R. Curry for providing the Gulf Stream and the Transport indices, respectively. The authors are grateful to the BCM group for help and guidance throughout the work. Support from the G. C. Rieber Foundations is also highly acknowledged. This is contribution No. A0041 from the Bjerknes Centre for Climate Research.

References

- Alley RB (1998) Paleoclimatology: Icing the North Atlantic. *Nature* 392 : 335–337
- Arakawa A, Lamb VR (1977) Computational Design of the Basic Dynamical Processes of the UCLA General Circulation Model. In: Chang J (ed) *Methods in Computational Physics*, volume 17, pp 173–265. Academic Press
- Bentsen M, Evensen G, Drange H, Jenkins AD (1999) Coordinate transformation on a sphere using conformal mapping. *Monthly Weather Review* 127 : 2733–2740
- Bentsen M, Drange H (2000) Parameterizing surface fluxes in ocean models using the NCEP/NCAR reanalysis data. In: *RegClim General Technical Report No. 4*, pp 149–158. Norwegian Institute for Air Research, Kjeller, Norway
- Bjerknes J (1964) Atlantic Air-Sea Interaction volume 10 of *Advances in Geophysics* pp 1–83. Academic Press
- Bleck R, Rooth C, Hu D, Smith LT (1992) Salinity-driven thermohaline transients in a wind- and thermohaline-forced isopycnic coordinate model of the North Atlantic. *J Phys Oceanogr* 22 : 1486–1515
- Bond G, Broecker W, Johnsen S, McManus J, Labeyrie L, J.Jouzel, G.Bonani (1993) Correlations between climate records from North Atlantic sediments and Greenland ice. *Nature* 365 : 143–147
- Bower A, Hunt H (2000) Lagrangian Observations of Deep Western Boundary Current in the North Atlantic Ocean. Part I: Large-Scale Pathways and Spreading Rates. *J Phys Oceanogr* 30 : 764–783
- Broecker WS (1997) Thermodynamic circulation, the achilles heel of our climate system: Will man-made CO₂ upset the current balance? *Science* 278 : 1582–1588
- Clark PU, Pisias NG, Stocker TF, Weaver AJ (2002) The role of the thermohaline circulation in abrupt climate change. *Nature* 415 : 863–869

- Covey C, AchutaRao KM, Cubasch U, Jones P, Lambert SJ, Mann ME, Phillips TJ, Taylor KE (2003) An overview of results from the Coupled Model Intercomparison Project. *Glob Planet Change* 37 : 103–133
- Cubasch U, Meehl GA, Boer GJ, Stouffer RJ, Dix M, Noda A, Senior CA, Raper S, Yap KS (2001) Projections of future climate change. In: Houghton JT, Ding Y, Nogua M, Griggs D, Linden PV, Maskell K (eds) *Climate Change 2001: The Scientific Basis*, pp 525–582. Cambridge University Press
- Curry R, McCartney MS (2001) Ocean Gyre Circulation Changes Associated with the North Atlantic Oscillation. *J Phys Oceanogr* 31 : 3374–3400
- Curry RG, McCartney MS, Joyce TM (1998) Oceanic transport of subpolar climate signals to mid-depth subtropical waters. *Nature* 391 : 575–577
- Delworth TL, Manabe S, Stouffer RJ (1993) Interdecadal Variations of the Thermohaline Circulation in a Coupled Ocean-Atmosphere Model. *J Climate* 6 : 1993–2011
- Delworth TL, Greatbatch RJ (2000) Multidecadal Thermohaline Circulation Variability Driven by Atmospheric Surface Flux Forcing. *J Climate* 13 : 1481–1495
- Déqué M, Dreveton C, Braun A, Cariolle D (1994) The ARPEGE/IFS atmosphere model: a contribution to the French community climate modelling. *Clim Dyn* 10 : 249–266
- Dickson B, Yashayaev I, Meincke J, Turrell B, Dye S, Holfort J (2002) Rapid freshening of the deep North Atlantic Ocean over the past four decades. *Nature* 416 : 832–837
- Dickson RR, Brown J (1994) The production of North Atlantic Deep Water: Sources, rates, and pathways. *J Geophys Res* 99 : 12319–12341
- Dickson RR, Lazier J, Meincke J, Rhines P, Swift J (1996) Long-term coordinated changes in the convective activity of the North Atlantic. *Prog Oceanog* 38 : 241–295
- Dixon KW, Delworth TL, Spelman MJ, Stouffer R (1999) The influence of transient surface fluxes on North Atlantic overturning in a coupled GCM climate change experiment. *Geophys Res Lett* 26 : 2749–2752

- Dong BW, Sutton RT (2001) The dominant mechanisms of variability in Atlantic ocean heat transport in a coupled ocean-atmosphere GCM. *Geophys Res Lett* 28 : 2445–2448
- Drange H, Simonsen K (1996) Formulation of air-sea fluxes in the ESOP2 version of MICOM. Technical Report 125, Nansen Environmental and Remote Sensing Center, Edv. Griegsv. 3A, N-5037 Solheimsviken, Norway
- Eden C, Jung T (2001) North Atlantic Interdecadal Variability: Oceanic Response to the North Atlantic Oscillation. *J Climate* 14 : 676–691
- Fichefet T, Gaspar P (1988) A Model Study of Upper Ocean-Sea Ice Interaction. *J Phys Oceanogr* 18 : 181–195
- Frankignoul C, de Coëtlogon G, Joyce TM, Dong S (2001) Gulf Stream Variability and Ocean–Atmosphere Interactions. *J Phys Oceanogr* 31 : 3516–3529
- Frankignoul C, Kestenare E, Botzet M, Carril AF, Drange H, Pardaens A, Terray L, Sutton R (2003) An intercomparison between the surface heat flux feedback in five coupled models, COADS and the NCEP reanalysis. *Clim Dyn.* submitted
- Friedrich H, Levitus S (1972) An Approximation to the Equation of State for Sea Water, Suitable for Numerical Ocean Models. *J Phys Oceanogr* 2 : 514–517
- Furevik T, Bentsen M, Drange H, Kindem IKT, Kvamstø NG, Sorteberg A (2003) Description and evaluation of the Bergen climate model: ARPEGE coupled with MICOM. *Clim Dyn* 21 : 27–51
- Gargett AE (1984) Vertical eddy diffusivity in the ocean interior. *J Mar Res* 42 : 359–393
- Gaspar P, Grégoris Y, Lefevre JM (1990) A Simple Eddy Kinetic Energy Model for Simulations of the Oceanic Vertical Mixing: Tests at Station Papa and Long-Term Upper Ocean Study Site. *J Geophys Res* 95 : 16179–16193
- Gent PR (2001) Will the North Atlantic Ocean thermohaline circulation weaken during the 21st century? *Geophys Res Lett* 28 : 1023–1026

- Gloersen P, Campbell WJ, Cavalieri DJ, Comiso JC, Parkinson CL, Zwally HJ (1992) Arctic and Antarctic Sea Ice, 1978–1987. National Aeronautics and Space Administration, Washington, D.C. NASA SP-551, 290 pp
- Griffies SM, Tziperman E (1995) A Linear Thermohaline Oscillator Driven by Stochastic Atmospheric Forcing. *J Climate* 8 : 2440–2453
- Hall MM, Bryden HL (1982) Direct estimates and mechanisms of ocean heat transport. *Deep-Sea Res* 29 : 339–359
- Hansen B, Turrell WR, Østerhus S (2001) Decreasing overflow from the Nordic seas into the Atlantic Ocean through the Faroe Bank channel since 1950. *Nature* 411 : 927–930
- Harder M (1996) Dynamik, Rauigkeit und Alter des Meereises in der Arktis. PhD thesis Alfred-Wegener-Institut für Polar- und Meeresforschung, Bremerhaven, Germany. 124 pp
- Hibler III WD (1979) A Dynamic Thermodynamic Sea Ice Model. *J Phys Oceanogr* 9 : 815–846
- Hurrell JW (1995) Decadal Trends in the North Atlantic Oscillation: Regional Temperatures and Precipitation. *Science* 269 : 676–679
- Jayne S, Marotzke J (2001) The dynamics of ocean heat transport variability. *Rev Geophys* 39 : 385–411
- Johnson HL, Marshall DP (2002) A theory for the surface Atlantic response to thermohaline variability. *J Phys Oceanogr* 32 : 1121–1132
- Joyce TM, Deser C, Spall MA (2000) The Relation between Decadal Variability of Subtropical Mode Water and the North Atlantic Oscillation. *J Climate* 13 : 2550–2569
- Kalnay E et al. (1996) The NCEP/NCAR 40-Year Reanalysis Project. *Bull Amer Meteor Soc* 77 : 437–471
- Kawase M (1987) Establishment of Deep Ocean Circulation Driven by Deep-Water Production. *J Phys Oceanogr* 17 : 2294–2317

- Latif M, Roeckner E, Mikolajewicz U, Voss R (2000) Tropical Stabilisation of the Thermohaline Circulation in a Greenhouse Warming Simulation. *J Climate* 13 : 1809–1830
- Lavin, Bryden HL, Parrilla G (1998) Meridional transport and heat flux variations in the subtropical North Atlantic. *The Global Ocean System* 6 : 269–293
- Levitus S, Boyer TP (1994) *World Ocean Atlas 1994 Volume 4: Temperature*. NOAA Atlas NESDIS 4, U.S. Department of Commerce, Washington, D.C. 117 pp
- Levitus S, Burgett R, Boyer TP (1994) *World Ocean Atlas 1994 Volume 3: Salinity*. NOAA Atlas NESDIS 3, U.S. Department of Commerce, Washington, D.C. 99 pp
- Mann ME, Park J (1994) Global-scale modes of surface temperature variability on inter-annual to century timescales. *J Geophys Res* 99 : 25819–25833
- Marshall J, Kushnir Y, Battisti D, Chang P, Czaja A, Dickson R, Hurrell J, McCartney M, Saravanan R, Visbeck M (2001) North Atlantic Climate Variability: Phenomena, Impacts and Mechanisms. *Int J Climatol* 21 : 1863–1898
- Mauritzen C, Häkkinen S (1999) On the relationship between dense water formation and the “Meridional Overturning Cell” in the North Atlantic Ocean. *Deep-Sea Res* 46 : 877–894
- McDougall TJ, Dewar WK (1998) Vertical Mixing and Cabbeling in Layered Models. *J Phys Oceanogr* 28 : 1458–1480
- Mikolajewicz U, Voss R (2000) The role of the individual air-sea flux components in CO₂-induced changes of the ocean circulation and climate. *Clim Dyn* 16 : 627–642
- O’Neill BC, Oppenheimer M (2002) Dangerous climate impacts and the Kyoto Protocol. *Science* 296 : 1971–1972
- Otterå OH, Drange H, Bentsen M, Kvamstø NG, Jiang D (2003a) The sensitivity of the present-day Atlantic meridional overturning circulation to freshwater forcing. *Geophys Res Lett* 30 : doi:10.1029/2003GL017578

- Otterå OH, Drange H, Bentsen M, Kvamstø NG, Jiang D (2003b) Transient response of enhanced freshwater to the Nordic Seas-Arctic Ocean in the Bergen Climate Model. *Tellus*. In press
- Parkinson CL, Washington WM (1979) A Large-Scale Numerical Model of Sea Ice. *J Geophys Res* 84 : 311–337
- Pickart RS, Straneo F, Moore GWK (2003) Is Labrador Sea Water formed in the Irminger basin? *Deep-Sea Res* 50 : 23–52
- Pickart R, Lavender K (2000) Is Labrador Sea Water Formed in the Irminger Basin? *WOCE Newsletter* 39 : 6–8
- Rahmstorf S, Ganopolski A (1999) Long-term global warming scenarios computed with an efficient coupled climate model. *Climate Change* 43 : 353–367
- Rosby T, Benway RL (2000) Slow variations in mean path of the Gulf Stream east of Cape Hatteras. *Geophys Res Lett* 27 : 117–120
- Schmittner A, Weaver AJ (2001) Dependence of multiple climate states on ocean mixing parameters. *Geophys Res Lett* 28 : 1027–1030
- Semtner Jr. AJ (1976) A Model for the Thermodynamic Growth of Sea Ice in Numerical Investigations of Climate. *J Phys Oceanogr* 6 : 379–389
- Smolarkiewicz PK (1984) A Fully Multidimensional Positive Definite Advection Transport Algorithm with Small Implicit Diffusion. *J Comput Phys* 54 : 325–362
- Smolarkiewicz PK, Clark TL (1986) The Multidimensional Positive Definite Advection Transport Algorithm: Further Development and Applications. *J Comput Phys* 67 : 396–438
- Stocker TF, Schmittner A (1997) Influence of CO₂ emission rates on the stability of the thermohaline circulation. *Nature* 388 : 862–865
- Sun S, Bleck R (2001) Thermohaline Circulation Studies with an Isopycnic Coordinate Ocean Model. *J Phys Oceanogr* 31 : 2761–2782

- Taylor AH, Stephens JA (1980) Latitudinal displacements of the Gulf Stream (1966 to 1977) and their relation to changes in temperature and zooplankton abundance in the NE Atlantic. *Oceanol Acta* 3 : 145–149
- Terray L, Thual O (1995) Oasis: le couplage océan–atmosphère. *La Météorologie* 10 : 50–61
- Terray L, Thual O, Belamari S, Déqué M, Dandin P, Lévy C, Delecluse P (1995) Climatology and interannual variability simulated by the arpege–opa model. *Clim Dyn* 11 : 487–505
- Timmermann A, Latif M, Voss R, Grötzner A (1998) Northern Hemispheric Interdecadal Variability: A Coupled Air-Sea Mode. *J Climate* 11 : 1906–1931
- Trenberth KE, Caron JM (2001) Estimates of Meridional Atmosphere and Ocean Heat Transports. *J Climate* 14 : 3433–3443
- von Storch JS, Müller P, Stouffer RJ, Voss R, Tett SFB (2000) Variability of Deep-Ocean Mass Transport: Spectral Shapes and Spatial Scales. *J Climate* 13 : 1916–1935
- Weaver AJ, Marotzke J, Cummins PF, Sarachik ES (1993) Stability and Variability of the Thermohaline Circulation. *J Phys Oceanogr* 23 : 39–60
- Weaver AJ, Sarachik ES (1991) Evidence for Decadal Variability in an Ocean General Circulation Model: An Advective Mechanism. *Atmos-Ocean* 29 : 197–231
- Weaver AJ, Sarachik ES, Marotzke J (1991) Freshwater flux forcing and interdecadal ocean variability. *Nature* 353 : 836–838
- Weaver AJ, Valcke S (1998) On the Variability of the Thermohaline Circulation in the GFDL Coupled Model. *J Climate* 11 : 759–767
- Weisse R, Mikolajewicz U, Maier-Reimer E (1994) Decadal variability of the North Atlantic in an ocean general circulation model. *J Geophys Res* 99 : 12411–12421
- Wood RA, Keen AB, Mitchell JFB, Gregory JM (1999) Changing spatial structure of the thermohaline circulation in response to atmospheric CO₂ forcing in a climate model. *Nature* 399 : 572–575

Wu P, Wood R, Stott P (2003) Does the recent freshening trend in the North Atlantic indicate a weakening thermohaline circulation? *Geophys Res Lett*. In press

Yang J (1999) A linkage between decadal climate variations in the Labrador Sea and the tropical Atlantic Ocean. *Geophys Res Lett* 26 : 1023–1026

Zalesak ST (1979) Fully Multidimensional Flux-Corrected Transport Algorithms for Fluids. *J Comput Phys* 31 : 335–362

List of Tables

1	Layer densities in σ_0 -units.	36
---	---	----

List of Figures

- 1 Annual mean AMOC from the ocean-only integrations for the the period 1948–1999 (top) and from the 300 years BCM control integration (bottom). The four ocean-only members are shown as dashed lines with the ensemble mean as solid thick line. 37
- 2 Top panels show the first EOF of the Atlantic overturning stream function (Sv) of the ensemble mean of the ocean-only simulations (left) and the BCM simulation (right). Bottom panels are the corresponding first PCs, where for each of the ocean-only simulations the PCs are shown as dashed lines with the ensemble mean as solid thick line. Note that the time spans of the axes are respectively 52 and 300 years. 38
- 3 The thick solid line denotes the spectrum of the leading PC of Atlantic overturning stream function in BCM, obtained using a Tukey-Hanning window with a width of 100 years. The thin solid line is a theoretical red noise spectrum found by fitting a first order autoregressive process. The dashed lines are the 95% confidence limits about the red noise spectrum. 39
- 4 The shading shows the areas in the ocean-only simulations (left) and the BCM simulation (right) where the mean February to April mixed-layer depth exceeds 1500 m at least once during the simulations. In the left panel, the different shadings indicate how many of the realizations that experience deep convective mixing at each location, going from light shaded (one realization) to dark shaded (all four realizations). 40
- 5 The annual cycle in the ML depth in the selected regions (see Fig. 4) for the ensemble-mean of the ocean-only simulations (top left) and the coupled simulation (top right). Annual cycle in the interannual variability of the ML depth, here represented as standard deviations for each month, are presented in the lower panels. Labrador Sea is shown as solid line, Irminger Sea as dashed line, and GIN Seas as dotted line. 41

6	Cross-correlation between convective mixing indices for the ensemble mean of the ocean-only simulations (left) and BCM (right). Positive lag indicates that the first location in the legend, lags the second. The v-shaped dashed lines indicate the 95% significance level.	42
7	Cross-correlation between convective mixing index and PC1 of Northern Hemisphere SLP (calculated from 20–80°N) for ensemble mean of ocean-only simulations (left) and coupled simulation (right). Positive lag means that the SLP PC1 lags the convective mixing. The v-shaped dashed lines indicate the 95% significance level.	43
8	Cross-correlation between the convective mixing indices and PC1 of the AMOC for the ensemble mean of the ocean-only simulations (left) and BCM (right). The time series have been high-pass filtered with a third order Butterworth filter with cut-off frequency $1/100 \text{ yr}^{-1}$. Positive lag means that the overturning lags the convective mixing. The v-shaped dashed lines indicate the 95% significance level.	44
9	Correlations between total heat flux anomalies (positive downwards, left panel) and the convective mixing index in the coupled integration for the Labrador Sea. The same analysis with SLP is shown in the right panel. Both heat flux and SLP are November through April averages. The time series have been band-pass filtered with a third order Butterworth filter using cut-off frequencies at $1/100$ and $1/5 \text{ yr}^{-1}$. The light shaded area indicates the 95% significance level. Positive (negative) correlations are given by solid (dashed) lines. Contour intervals are 0.25, 0.4 and 0.6, with increasing thickness of the contour lines with increasing correlations. . .	45
10	As Fig. 9, but with the convective mixing index for the Irminger Sea. . .	46

11	<p>Mixing indices for the Irminger Sea (thin line) and the Labrador Sea (thin dashed line), together with the leading PC of the AMOC (thick line). The top panel shows the ensemble mean time series from the ocean-only simulations, while the three lower panels are from the BCM simulation. The time series have been high-pass filtered with a third order Butterworth filter with cut-off frequency $1/100 \text{ yr}^{-1}$, smoothed with a 3 year running mean, and finally normalized. The two convective mixing indices have been shifted 4 years forward in time to better match the PC of the AMOC.</p>	47
12	<p>The location of the vertical sections used in Figs. 13 (left panel) and 14 (right panel). The sections end where the arrow is drawn. In Fig. 13, the velocity is directed along the section, with positive correlations indicating anomalous southward flows. In Fig. 14, the velocity is normal to the section, with positive correlations indicating anomalous northward flows.</p>	48
13	<p>Lag correlations between potential density (first column), temperature (second column), salinity (third column), and velocity (forth column) along the section shown in the left panel of Fig. 12, and the leading PC of the AMOC from the BCM experiment. The time series have been band-pass filtered with a third order Butterworth filter with cut-off frequencies $1/100$ and $1/5 \text{ yr}^{-1}$. The light shaded area indicates the 95% significance level. Positive (negative) correlations are given by solid (dashed) lines. Contour intervals are 0.25, 0.4 and 0.6 with increasing thickness of the contour lines. The lags (in years, positive when AMOC is leading) are indicated in the lower left corner of the panels. Section length (depth) is 7943km (4500m).</p>	49
14	<p>As Fig. 13, but for the section along 48°N, see Fig. 12. Section length (depth) is 3868km (4000m).</p>	50
15	<p>Lag correlations between the barotropic stream function and PC1 of AMOC in the BCM experiment. Filtering, contouring and significance as for Fig. 9.</p>	51
16	<p>Lag correlations between the $\sigma_0 = 27.71$ interface depth anomalies and PC1 of the AMOC. Filtering, contouring and significance as for Fig. 9.</p>	52

17	Ensemble mean of the leading PCs of the AMOC (solid line) and Atlantic tropical dipole index (dashed line) from the ocean-only simulations. The time series have been high-pass filtered with a third order Butterworth filter with cut-off frequency $1/20 \text{ yr}^{-1}$. The overturning PC is leading the dipole index by 6 years, and both time series have been smoothed with a 5 year running mean.	53
18	Top panel: Ensemble mean of the first PCs of the Atlantic overturning stream function from the ocean-only simulations (solid line) and the Atlantic Transport Index (open circles) as defined in Curry and McCartney (2001). Middle panel: The Gulf Stream index for each of the ocean-only simulations (dashed lines) and the ensemble mean of the four members (solid line). Lower panel: The simulated ensemble mean Gulf Stream index (solid line, and the same as shown in the mid panel), together with the Gulf Stream index constructed from XBT data at 200 m during 1954–98 as used in Frankignoul et al. (2001) (dashed line).	54
19	Left panel: The difference in SLP (mbar) in the BCM experiment for the months November-April for the composite of years with the PC1 of the AMOC exceeding one standard derivation (15 years) and receding one standard derivation (10 years). Long term variability has been removed from the AMOC time series prior to the analysis. Right panel: As for the left panel, but for 2 m temperature ($^{\circ}\text{C}$).	55

Layer	σ_0	Layer	σ_0	Layer	σ_0	Layer	σ_0
1		7	26.52	13	27.63	19	27.94
2	24.12	8	26.80	14	27.71	20	27.98
3	24.70	9	27.03	15	27.77	21	28.01
4	25.28	10	27.22	16	27.82	22	28.04
5	25.77	11	27.38	17	27.86	23	28.07
6	26.18	12	27.52	18	27.90	24	28.10

Table 1:

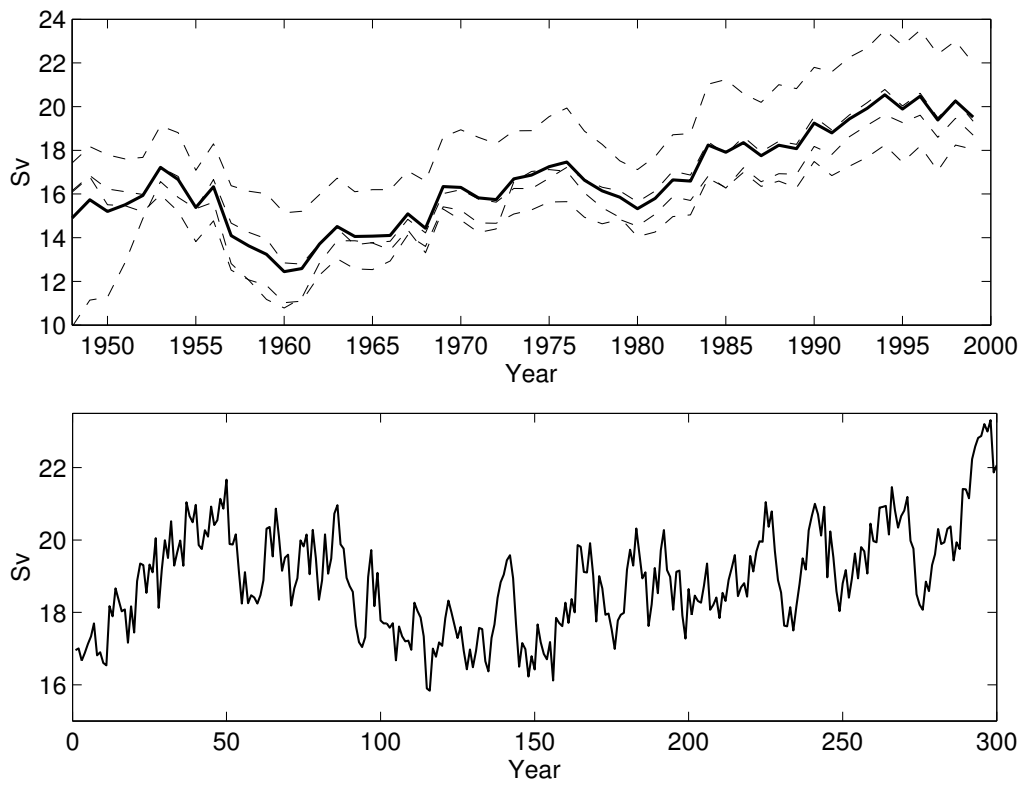


Figure 1:

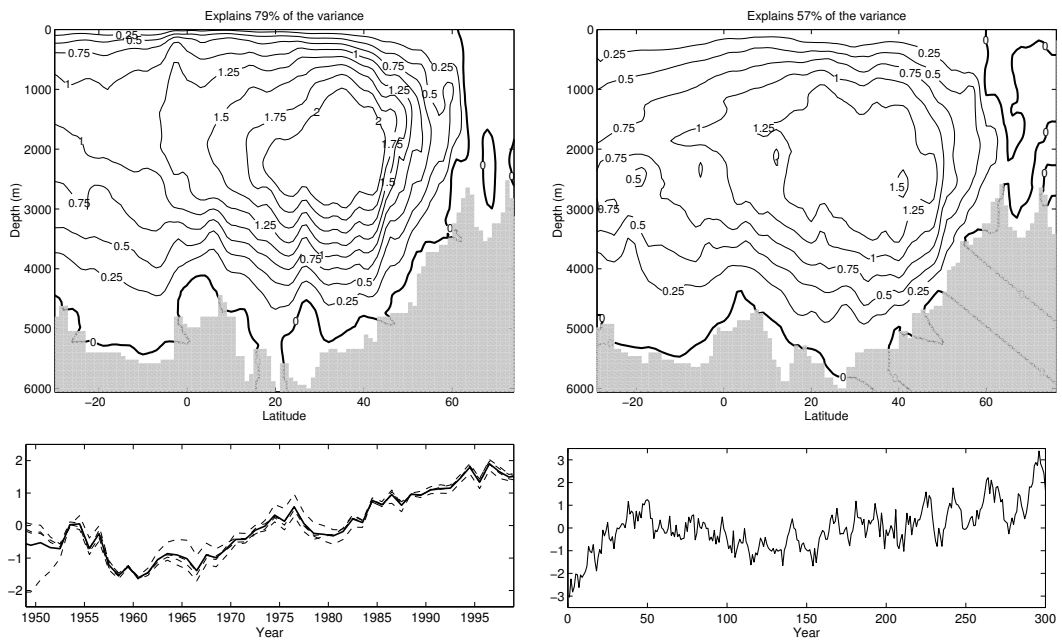


Figure 2:

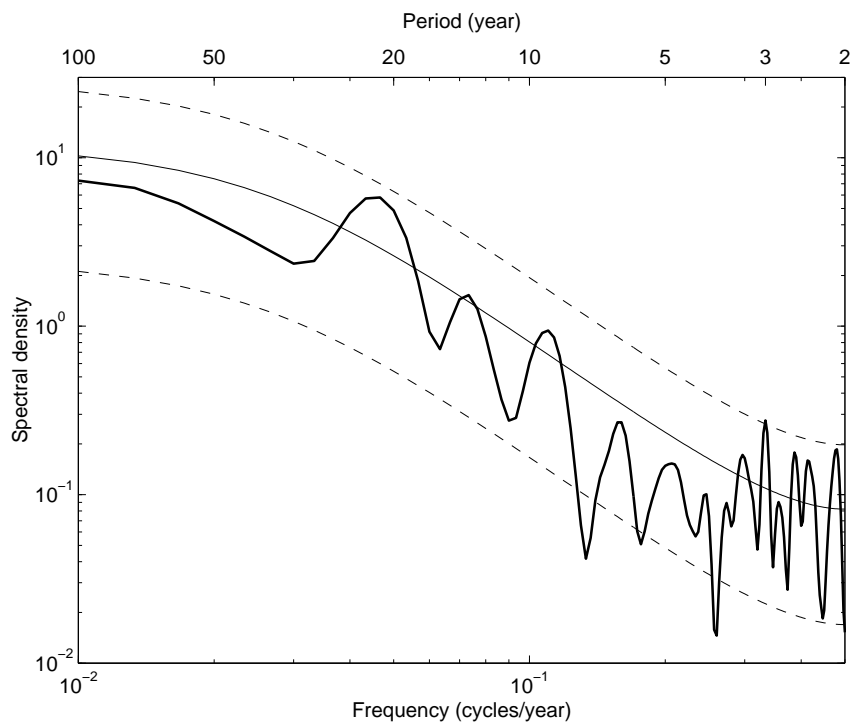


Figure 3:

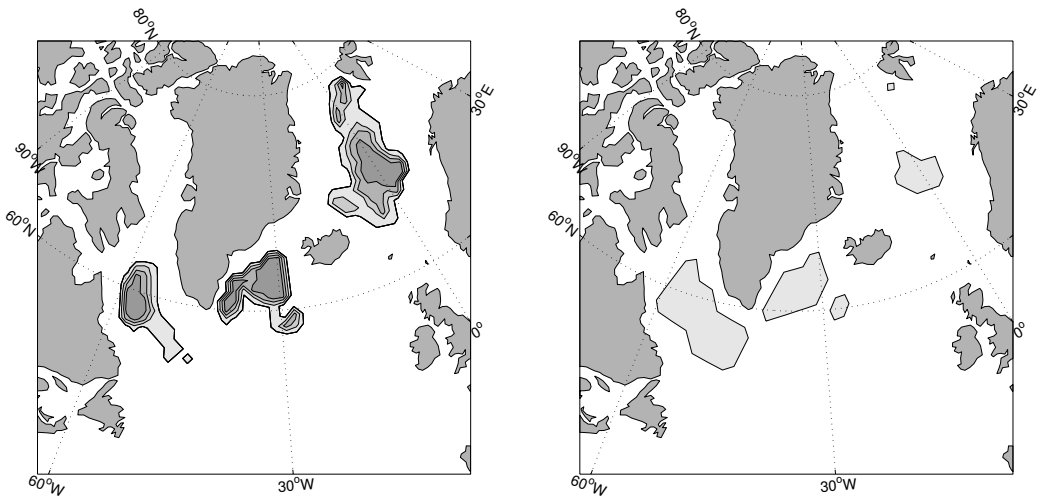


Figure 4:

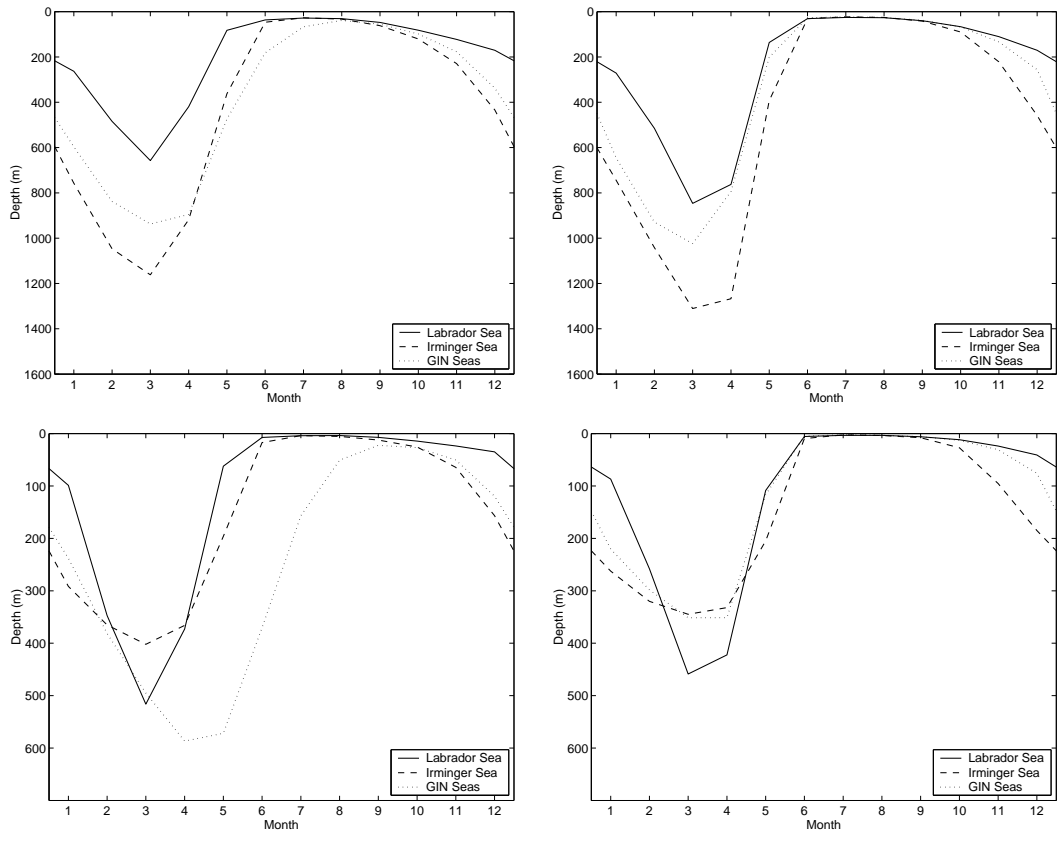


Figure 5:

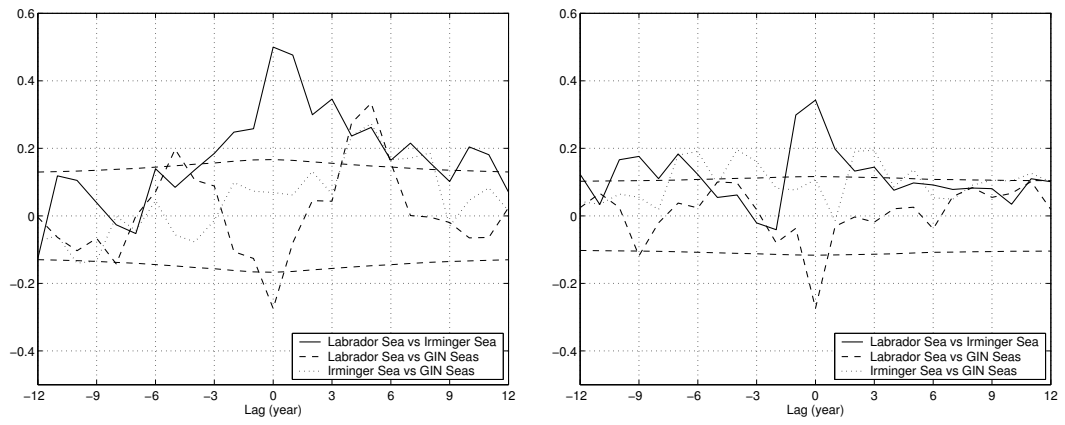


Figure 6:

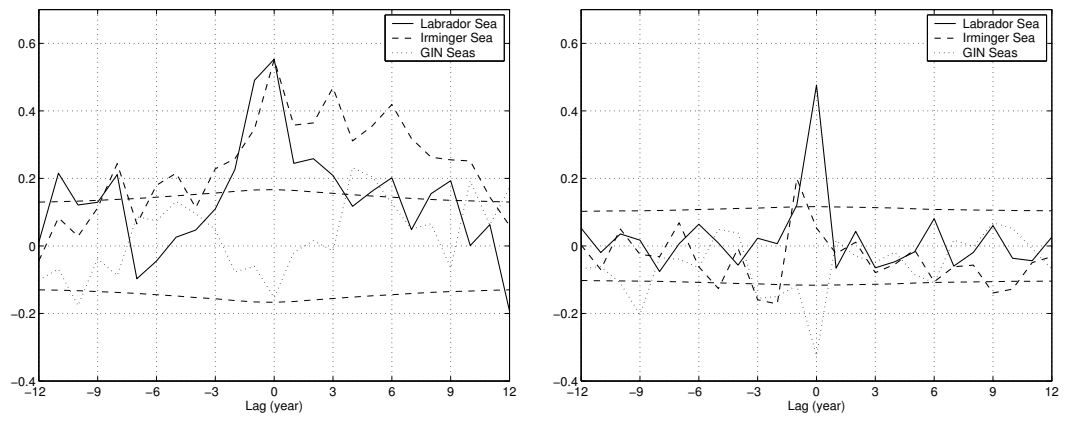


Figure 7:

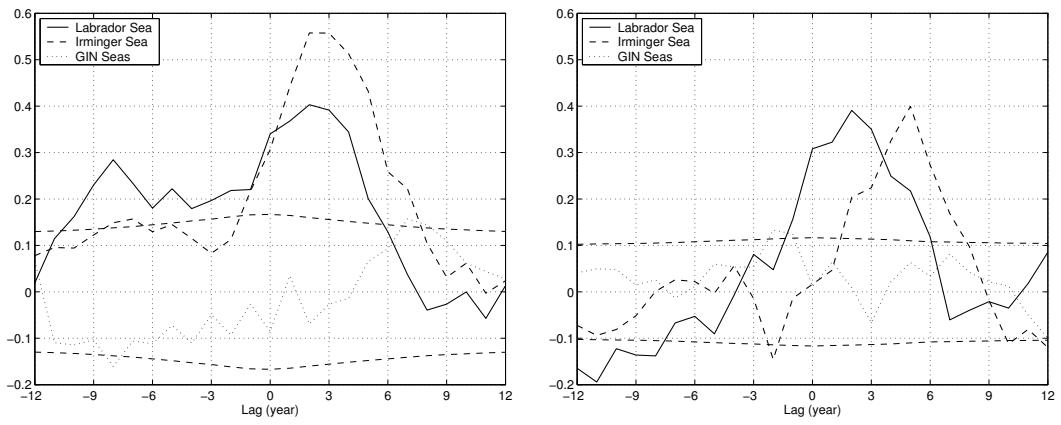


Figure 8:

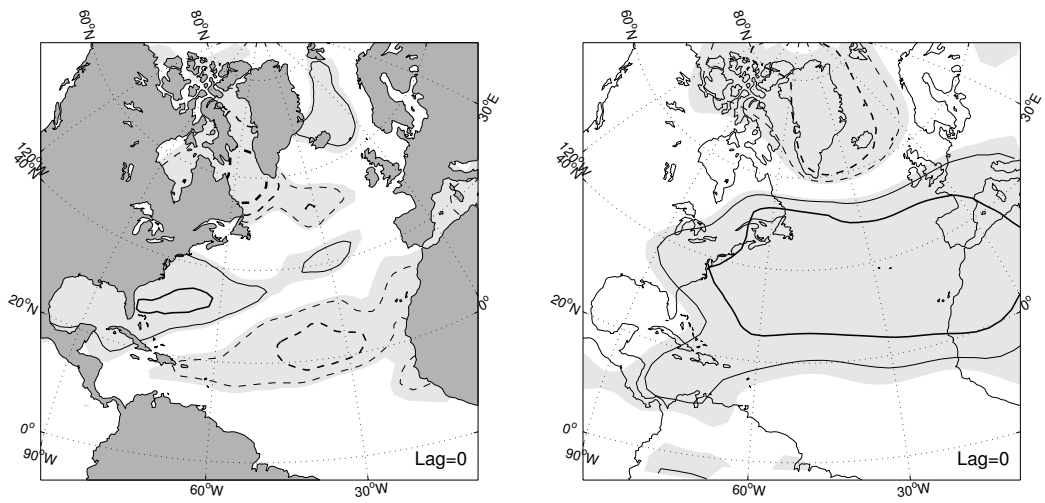


Figure 9:

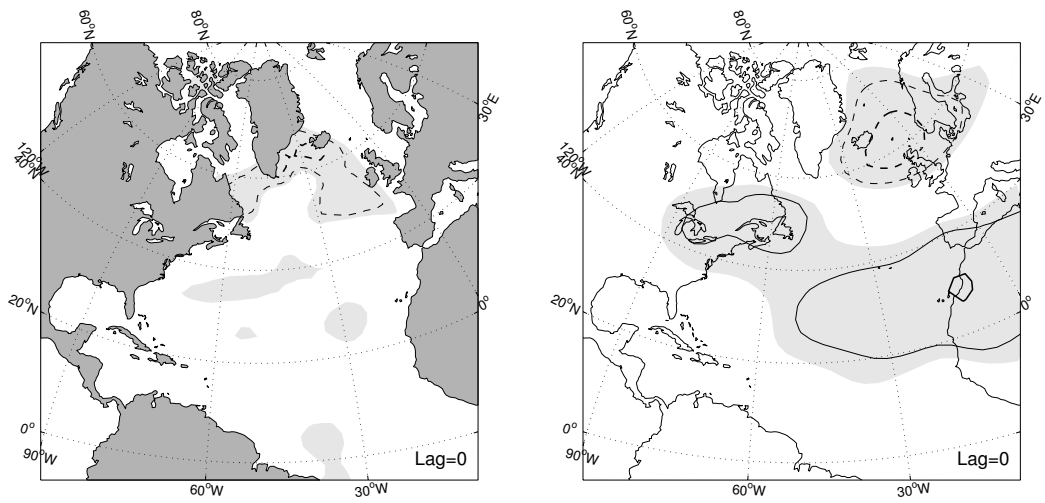


Figure 10:

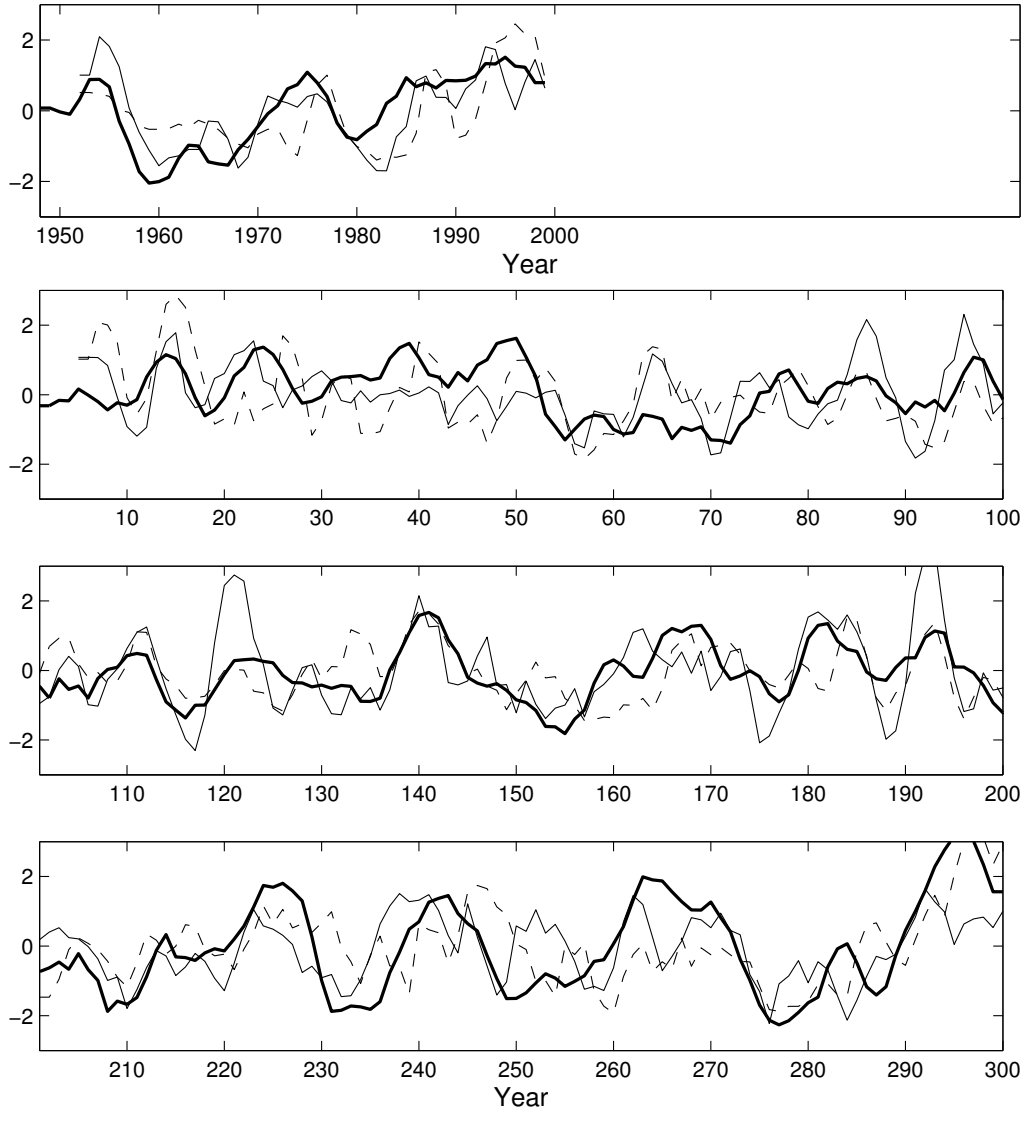


Figure 11:

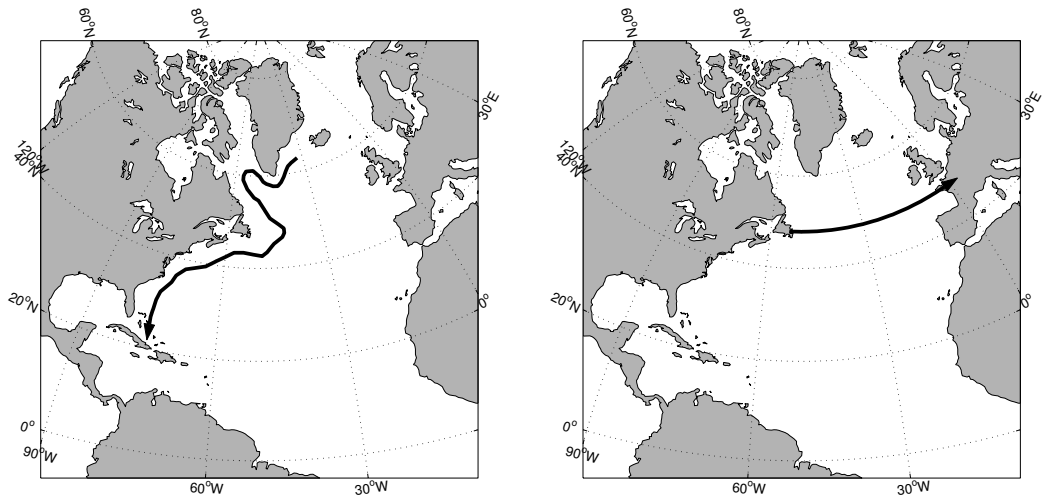


Figure 12:

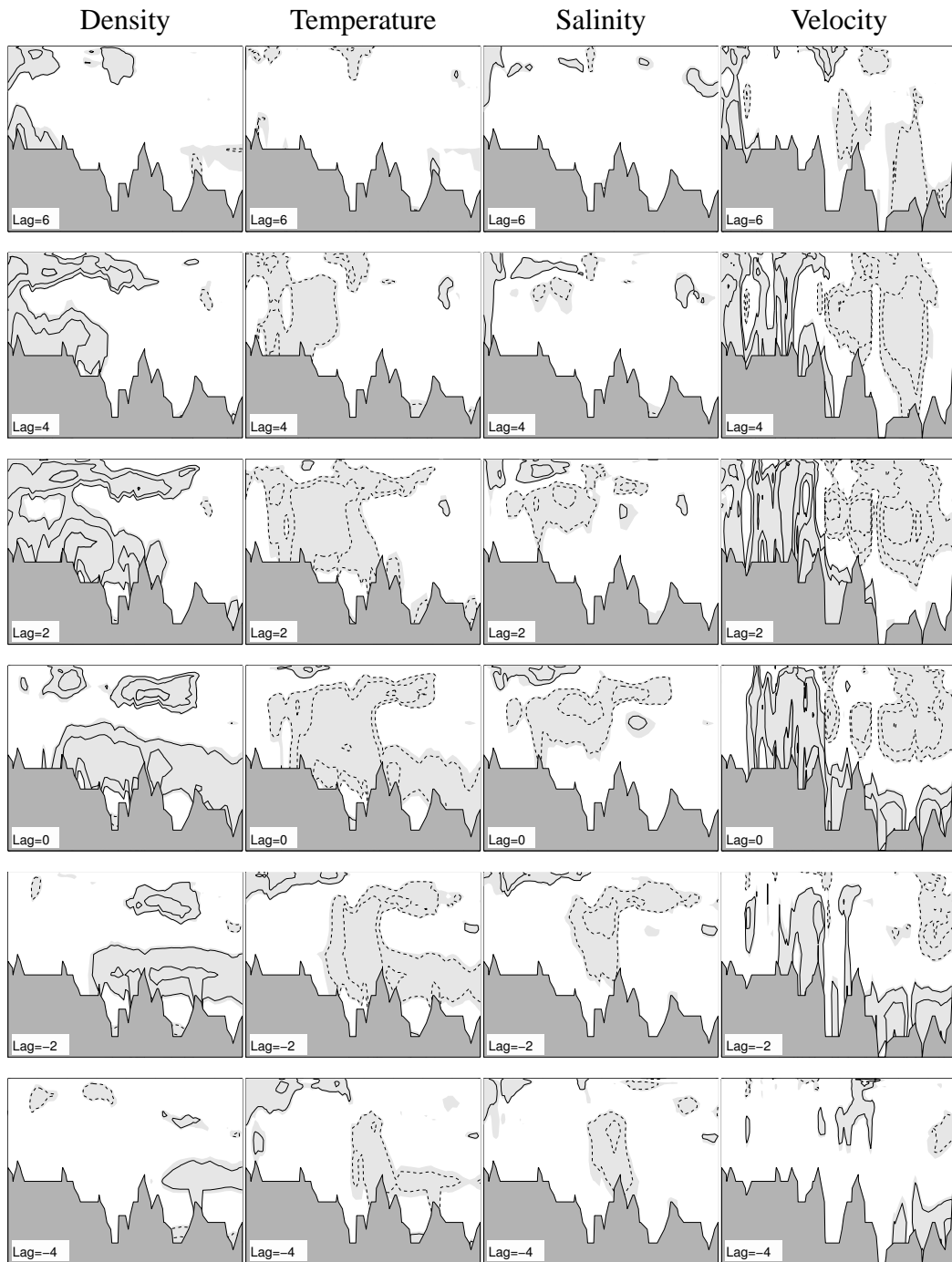


Figure 13:

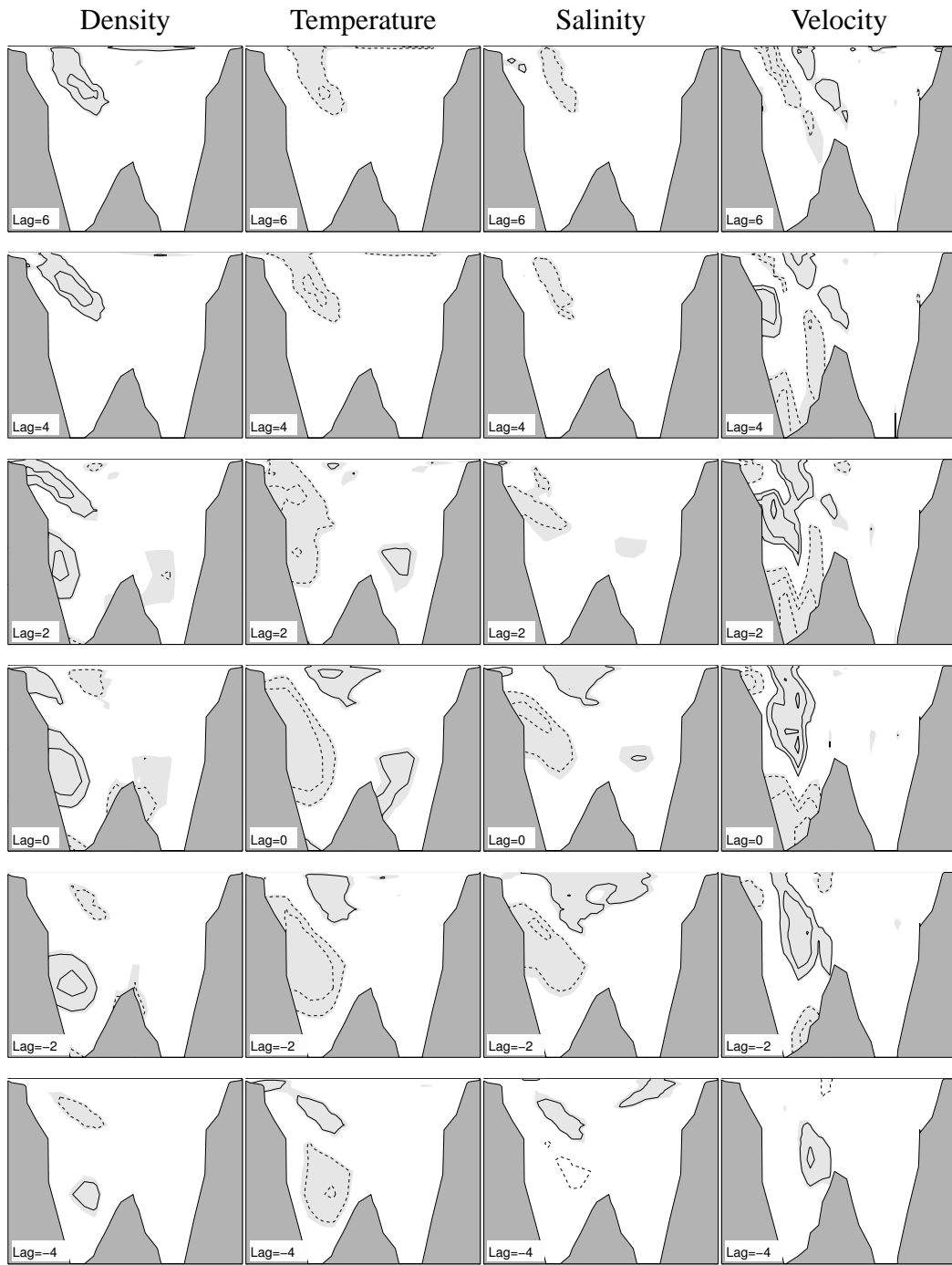


Figure 14:

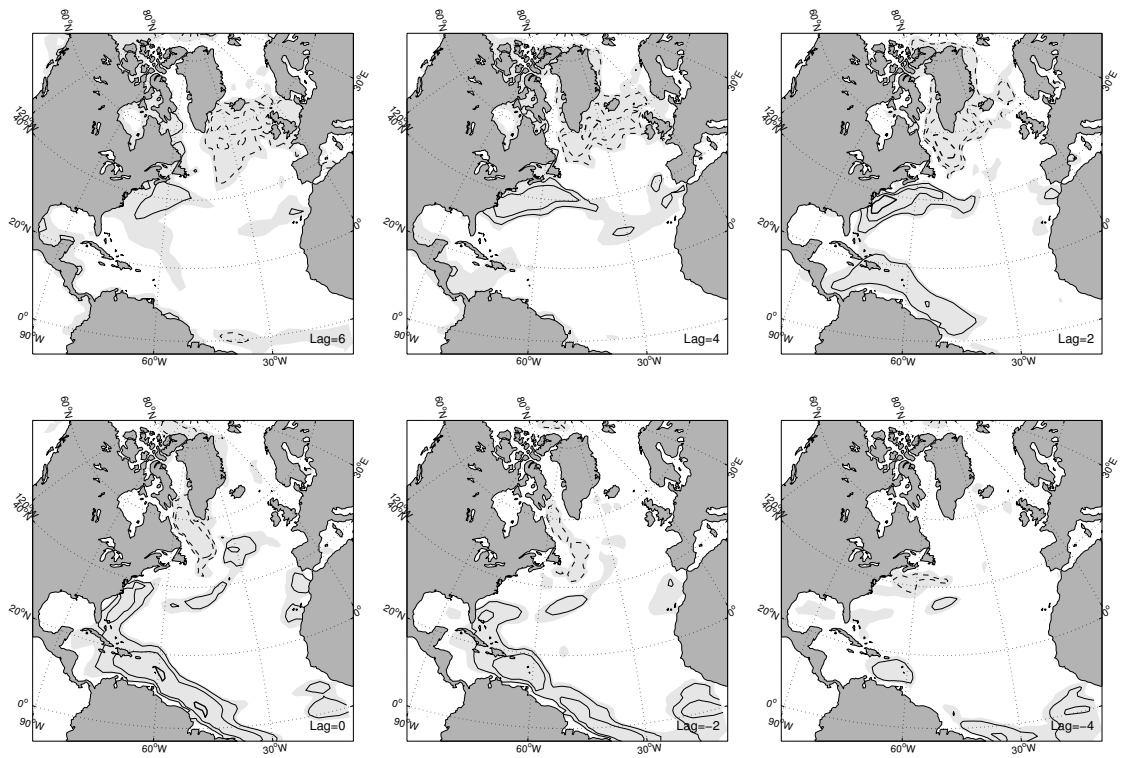


Figure 15:

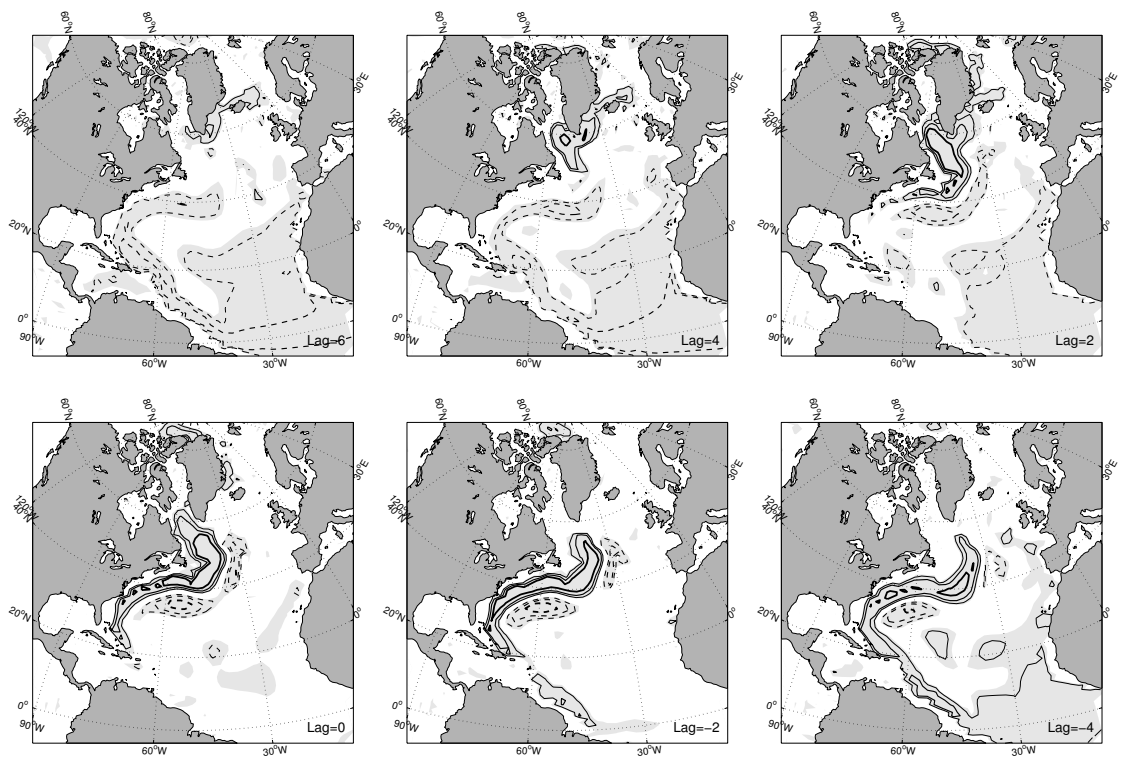


Figure 16:

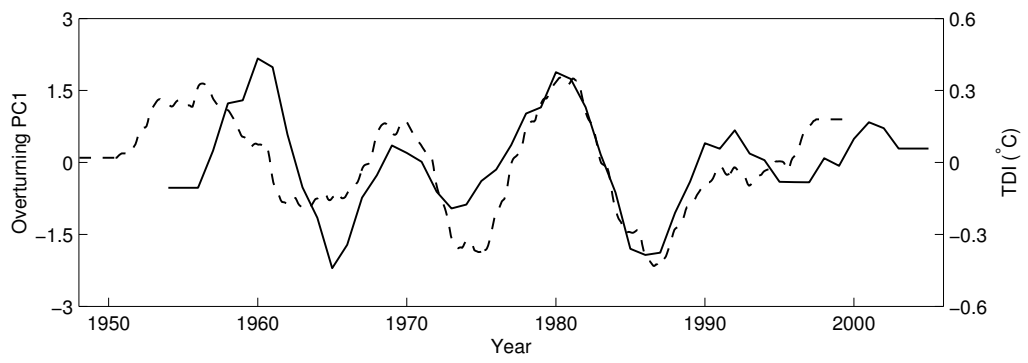


Figure 17:

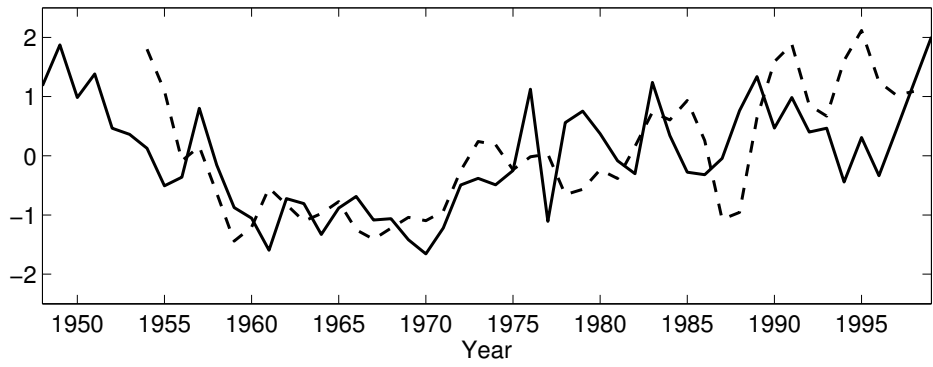
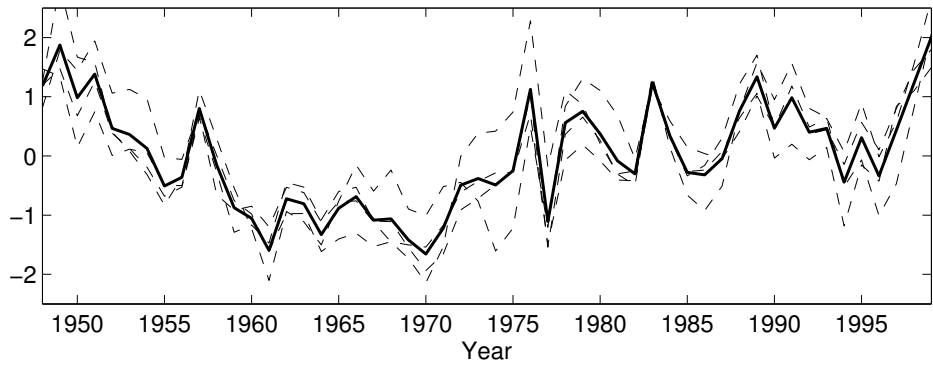
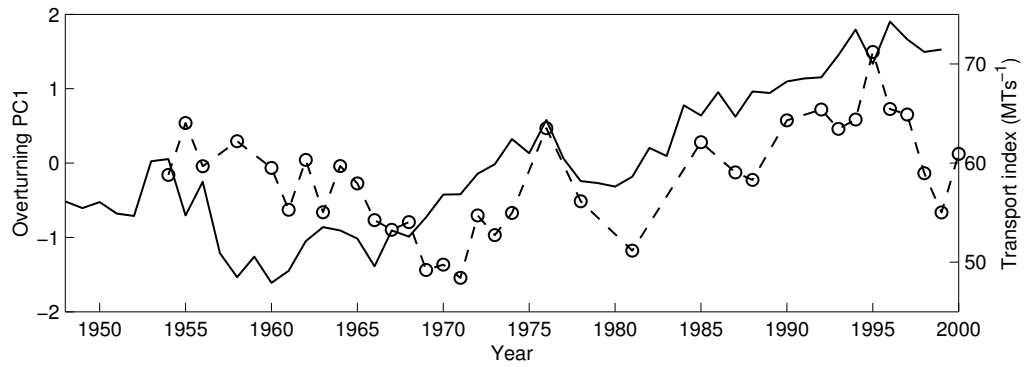


Figure 18:

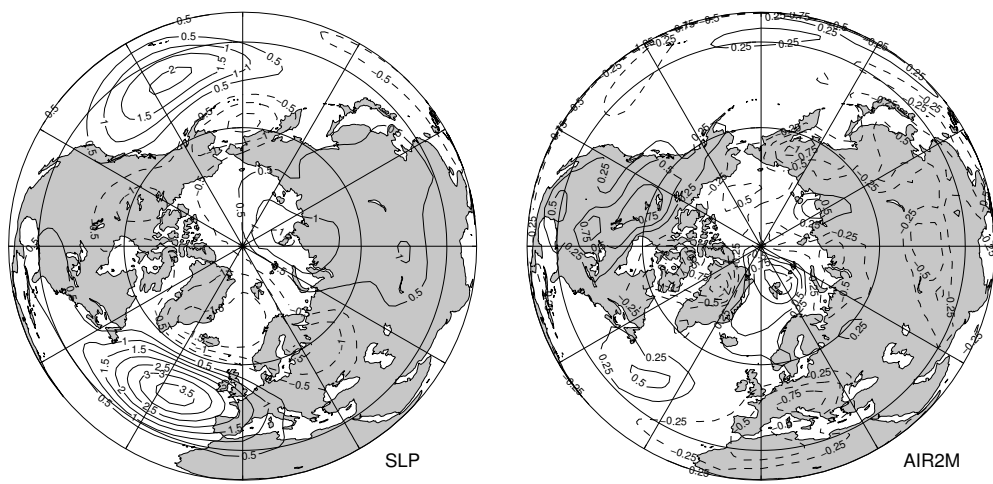


Figure 19: